View metadata, citation and similar papers at core.ac.uk

brought to you by CORE

provided by Cleveland-Marshall College of Law

Cleveland State University
EngagedScholarship@CSU

ETD Archive

2009

Non-Collocation Problems in Dynamics and Control of Mechanical Systems

Timothy M. Obrzut
Cleveland State University

Follow this and additional works at: https://engagedscholarship.csuohio.edu/etdarchive


Part of the Mechanical Engineering Commons

How does access to this work benefit you? Let us know!

Recommended Citation

Obrzut, Timothy M., "Non-Collocation Problems in Dynamics and Control of Mechanical Systems" (2009). *ETD Archive*. 665.
https://engagedscholarship.csuohio.edu/etdarchive/665

This Thesis is brought to you for free and open access by EngagedScholarship@CSU. It has been accepted for inclusion in ETD Archive by an authorized administrator of EngagedScholarship@CSU. For more information, please contact library.es@csuohio.edu.

NON-COLLOCATION PROBLEMS IN DYNAMICS AND CONTROL OF MECHANICAL SYSTEMS

TIMOTHY M. OBRZUT

Bachelor of Science in Mechanical Engineering

The Ohio State University

June, 2002

Submitted in partial fulfillment of requirements for the degree

MASTER OF SCIENCE IN MECHANICAL ENGINEERING

at the

CLEVELAND STATE UNIVERSITY

December, 2009

This thesis has been approved
for the Department of MECHANICAL ENGINEERING
and the College of Graduate Studies by

Dr. Jerzy T. Sawicki, Thesis Committee Chairperson
Department of Mechanical Engineering, CSU

Dr. John L. Frater
Department of Mechanical Engineering, CSU

Dr. Ana V. Stankovic
Department of Electrical and Computer Engineering, CSU

ACKNOWLEDGEMENTS

I would like to thank Dr. Jerzy T. Sawicki for his role as advisor. He always found the time despite his busy schedule to answer my questions and to help solve problems. Without his vast knowledge and guidance, this work would not have been possible. I would also like to thank Dr. John L. Frater and Dr. Ana V. Stankovic, who served on the thesis committee, for their time, counsel, and evaluation.

I would also like to thank my employer, MTD Products for providing financial support and also time throughout the day to complete my work.

NON-COLLOCATION PROBLEMS IN DYNAMICS

AND CONTROL OF MECHANICAL SYSTEMS

TIMOTHY M. OBRZUT

ABSTRACT

Characteristics of mechanical systems with non-collocated sensors and actuators are investigated. Transfer function zeros location as a function of sensor position, zero-pole interlacing, and re-location of zeros are discussed in a context of presented examples. Some of the presented examples involving non-collocation are supported by experimental data. A case study involving a high speed machining spindle is examined. The control problems associated with non-collocation are studied along with the methods to solve them.

TABLE OF CONTENTS

NOMENCLATURE

a = mass eccentricity of unbalance $[m]$

A_{11} = row one, column one of stiffness matrix

A_{12} = row one, column two of stiffness matrix

A_{21} = row two, column one of stiffness matrix

A_{22} = row two, column two of stiffness matrix

b_1 = damping of damper one $\left[\frac{N-s}{m}\right]$

b_2 = damping of damper two $\left[\frac{N-s}{m}\right]$

b_3 = damping of damper three $\left[\frac{N-s}{m}\right]$

c_1 = damping of damper one $\left[\frac{N-s}{m}\right]$

c_2 = damping of damper two $\left[\frac{N-s}{m}\right]$

F_ϕ = constant magnitude force applied to mass one $[N]$

$G(1,1)$ = transfer function relating the front bearing to the front sensor $[non-\dim]$

$G(3,3)$ = transfer function relating the back bearing to the back sensor $[non-\dim]$

k_1 = stiffness of spring one $\left[\frac{N}{m}\right]$

k_2 = stiffness of spring two $\left[\frac{N}{m}\right]$

k_3 = stiffness of spring three $\left[\frac{N}{m}\right]$

K = stiffness ratio $[non-\dim]$

L = length of modified Jeffcott rotor $[m]$

m_1 = mass one $[kg]$

m_2 = mass two $[kg]$

$m_2\omega^2 a$ = unbalance force $\left[\frac{kg-m}{s^2}\right]$

M = mass ratio $[non-\dim]$

p_i = system poles $\left[\frac{rad}{s}\right]$

q_1 = displacement of mass one $[m]$

q_2 = displacement of mass two $[m]$

u = control force $[N]$

u_i = output deflection $[m]$

ω = frequency $\left[\frac{rad}{s}\right]$

ω_i = i^{th} resonant frequency $\left[\frac{rad}{s}\right]$

ω_{0i} = i^{th} anti-resonant frequency $\left[\frac{rad}{s}\right]$

x_1 = displacement of mass one $[m]$

x_2 = displacement of mass two $[m]$

$X(s)$ = harmonic output $\left[\frac{rad}{s}\right]$

y_i = input signal to the active magnetic bearing $\left[\frac{rad}{s}\right]$

$Y(s)$ = harmonic input $\left[\frac{rad}{s}\right]$

z_i = system zeros $\left[\frac{rad}{s}\right]$

z_s = axial location of sensor $[m]$

α = ratio between sensor offset and shaft half-span $[non-\dim]$

Ω = natural frequency normalized to critical speed of mass two $[non-\dim]$

LIST OF TABLES

LIST OF FIGURES

CHAPTER I

INTRODUCTION

1.1 Background and Motivation

Merriam Webster defines collocation as "the act or result of placing together." In the application of control systems the definition would be the act of placing the input force together with the sensor that controls the input force. All actively controlled mechanical systems are either collocated or non-collocated. When a sensor is placed at the same location as the input force, the system is said to be collocated. There are many reasons why this is the preferred method of sensors and actuators placement. These benefits will be discussed in the following chapters. However, in many real life mechanical systems, collocation is simply not possible and this presents some unique problems for system control. Some such cases include for example a high-speed machining spindle supported by active magnetic bearings [Sawicki 2006] or robotics

applications [Damaren 2000]. In both of these cases, the input force acts on the system at one point, and the sensor is measuring the response at another.

1.2 Literature Review

Structural engineers and control system designers know of the importance of natural frequencies, or poles, in a system. Generally more importance is placed on the poles than on the zeros of a particular system [Preumont 2002]. When the system in question is non-collocated, this can present the structural engineer or control system designer with many issues. Spector and Flashner [1989] investigated the sensitivity of a non-collocated structural model. They found that the zeros in a system are much more sensitive to perturbations in the system parameters and boundary conditions than the poles. Also, small variations in the sensor locations can result in interchanging the order of poles and zeros. This could result in closed-loop instability. These results were verified with a pinned-free beam model. Further work has been done on studying the beam model in a collocated case. Richolet [2004] investigated two control laws, position positive feedback and generalized predictive control. It was found that generalized predictive control was suitable for damping the first vibration mode.

Miu [1991] did work on providing a physical interpretation of the zeros. This work also showed the importance of zeros in ensuring the stability of control systems. Furthermore, it was found that the zeros of a collocated system are the resonances of a substructure constrained at the sensor and actuator location. This has the meaning that an additional constraint is introduced to a collocated sensor and actuator. This additional

constraint is not present in a non-collocated system. This is helpful in understanding why a collocated system would be stable and not a similar non-collocated system.

Loix [1996] investigated complex zeros of non-collocated systems. His work proved the existence of complex zeros in non-collocated systems. Through analyzing a simply supported beam and a four mass system he found the presence of complex zeros can increase the sensitivity of the control system to parameter variation. Furthermore, if these complex zeros occur within the operating range of the system, the system can become unstable.

Theoretical work has also been done on non-collocation with respect to an abstract second order system, [Guo 2008]. This work studied the stabilization of multi-dimensional wave equations under non-collocated control and observations. Four cases were investigated, locally internal distributed control and observation, internal distributed control and boundary observation, boundary control and internal distributed control and observation, and locally internal distributed control and boundary observation. This work was then applied to the Euler-Bernoulli beam equation, [Guo 2008]. The multiplier methods, Reisz basis approach, and the Lyapunov function were employed to analyze the stability of the partial differential equations. It was concluded that the multiplier method was not effective in proving the stability of the closed-loop system that was studied.

The flexible beam model has been employed to study a multitude of characteristics including non-collocation and control systems. Sun [2001] investigated partial debonding of piezoelectric sensors and actuators on a cantilevered flexible beam. The non-collocation control was achieved by using two piezoelectric patch pairs. The work centered on varying the amount of debonding in the collocated and non-collocated

cases. It was found that if the debonding was located at the end of the actuator or sensor, the controllability of the first several modes of the beam was significantly diminished. Furthermore, it was stated that a single actuator is much more sensitive to debonding than an actuator pair in the closed-loop vibration control of the beam.

Qiu [2009] also employed the cantilevered flexible beam model to study vibration suppression with non-collocated PZT actuator and accelerometer. Phase shifting technology was applied to the controller to account for the non-collocation effects. The proposed methods were effective in suppressing the first two bending modes of the beam.

Lacarbonara [2006] used a slender beam to investigate the effectiveness of a non-linear strategy for cancelling the parametrically forced skew-symmetric vibrations of a straight elastic beam via a non-collocated input. Two-frequency control signals were found to be effective in cancelling the resonances provided that the control gains were within certain theoretically determined bounds.

These ideas were further investigated in active magnetic bearings. Active magnetic bearings are inherently non-collocated [Sawicki 2007]. However, they are a promising new technology that offers many benefits to a wide range of industries. The most notable would be high-speed machining. Current high-speed machining is limited to about 15,000 rpm [Zelinski 2008] and active magnetic bearings would be able to increase this capability to 50,000 rpm [Sawicki 2008]. In order to realize these benefits, robust control systems are required. These robust control systems can only be developed once a good understanding of the model and non-collocation is achieved. Active magnetic bearings also present some other interesting challenges. These include accurate system modeling. Accurately modeling a real life system can be challenging because

there are difficulties in representing some features. One of these features is the shrink fits of the magnetic bearings, motor, and sensors to the rotor. While the mass can be easily calculated, the stiffness is more difficult to accurately predict. Another feature that is difficult to accurately represent is the laminations of the magnetic bearings and motor. These laminations are known to be very thin, approximately 0.1 mm and modeling each one individually is not a viable option. The motor is the third feature that proves to be challenging to accurately model. The motor consists of three different materials, steel, copper, and iron, thin laminations, and 30 copper rods pressed axially into the subassembly. Understanding the interactions between all these parts and accurately representing them in a model is challenging. Finally, the tool holder represents another source of potential inaccuracies. The end of the spindle is counter-bored and threaded. The tool holder fits into the counter-bore and is secured with a bolt. Representing the threaded connection with two different materials and understanding the effects on the stiffness is difficult. Some of these issues could be solved by creating a very detailed model. This would result in an extremely large model that might be too large to be of any practical value. Therefore, there must be a trade-off between the size of the model and the accuracy of the model. This issue is greatly magnified by non-collocation, because small inaccuracies can lead to qualitatively different system characteristics which can lead to inefficient or unstable control systems [Spector 1990].

Control strategies for non-collocated systems have also been investigated. Bruin [2008] looked into state feedback control systems for non-collocated mechanical motion systems with set-valued frictional nonlinearities. His work obtained input-to-state stability with respect to perturbations on the system studied. Nordstrom [2004] proposed

a time delay method to solve non-collocated input estimation problems. His work showed that introducing a time delay can improve the input estimation considerably. Buhr [1997] considered a non-collocated passive vibration absorber for vibration attenuation. The passive vibration absorber was found to be uncontrollable for certain frequencies. This was solved by developing a feedback based tuning algorithm for a variable stiffness vibration absorber.

1.3 Objectives of Thesis

It is important to understand the benefits of collocated systems and the drawbacks of non-collocated systems so that a control system designer can choose a collocated system if at all possible. In some cases, the control system designer has no choice and must use a non-collocated system. When this occurs, it is imperative that the effects of non-collocation are fully understood. With this better understanding, better and more accurate control systems can be designed and implemented. With accurate control systems widely available, technologies such as active magnetic bearings and robotics can be used in a wide range of industries. These technologies can lower cost and increase quality for many industries. This thesis will examine the differences between collocated and non-collocated systems by solving examples and by studying a non-collocated high-speed machining spindle.

1.4 Thesis Outline

This thesis will contain four main chapters. The second chapter will present the characteristics of a collocated system and the reasons why this is the preferred method of

sensor placement. This chapter will present examples to show the differences between collocated and non-collocated systems. The third chapter will describe an extended Jeffcott rotor supported on actively controlled magnetic bearings (AMBs). This will include the effect of non-collocation on the critical speeds. The fourth chapter will be devoted to a case study of a high-speed machining spindle running on AMBs. In this chapter, a specific high-speed machining spindle will be presented. A finite element (FE) model of the spindle rotor will be introduced with the accompanying analysis. The effects of non-collocation will be clearly shown. Finally, the fifth chapter will provide a summary and conclusions for the thesis and it will outline possible directions for future studies.

CHAPTER II

CHARACTERISTICS OF COLLOCATED VERSUS NON-COLLOCATED SYSTEMS

2.1 Introduction

One of the most important characteristics of any control system is stability. A collocated system is generally more stable to large perturbations of the system parameters than the same system without collocation. This is true due to the alternating poles and zeros that are present in collocated systems. Systems with alternating poles and zeros, also known as pole-zero interlacing, are stable [Preumont 2002]. Non-collocated systems might not have the property of pole-zero interlacing due to pole-zero flipping. Pole-zero flipping often lead to unstable systems [Preumont 2002]. These characteristics are shown in more detail in the examples in a later section of this chapter and the following chapter.

The phenomenon known as anti-resonance occurs between consecutive resonant frequencies in collocated systems. Bode diagrams plot the frequency response of a

system. The frequency response has two components, amplitude and phase. The Bode diagram plots the amplitude and phase of the response over a wide range of frequencies. The system natural frequencies, or poles, appear as peaks and the anti-resonant frequencies, or zeros, appear as negative peaks. While anti-resonance frequencies are not unique to collocated systems, they will always appear in collocated systems between consecutive resonant frequencies. The anti-resonant frequencies are the frequencies where the amplitude of the frequency response function (FRF) vanishes [Preumont 2002].

2.2 Transfer Functions

In the field of control systems, it is customary to write the dynamics of the system in terms of a transfer function. "The term 'transfer function' stems from the fact that by knowing $G(s)$ we may transfer any set of force amplitudes F into a response." [Ginsberg 2001].

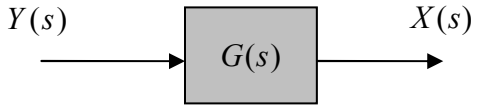

Figure 2.1 Block diagram of a single input and single output system

Figure 2.1 shows a simple block diagram that graphically demonstrates a transfer function. In this system, $Y(s)$ is the input and $X(s)$ is the output. The transfer function is $G(s)$. It should be noted that the input, output, and transfer function are complex quantities because they consist of an amplitude and phase. Equation (2.1) shows a generalized transfer function for the system in Fig. 2.1. This clearly shows that the transfer function is the ratio of the output of the system over the input of the system.

$$G(s) = \frac{X(s)}{Y(s)} \tag{2.1}$$

Depending on the number of inputs to the system and the number of outputs, a system can have numerous transfer functions.

Equation (2.1) is a generalized form of a transfer function for any given system. In the case of control systems, it is common to rewrite Eq. (2.1) as follows:

$$G(s) = k\frac{\prod_{zeros}(s - z_i)}{\prod_{poles}(s - p_i)} \tag{2.2}$$

The above equation is written in the Laplace domain and it shows the transfer function is a gain, k, multiplied by the system zeros and divided by the system poles. Furthermore, in the case of collocated systems without damping, Eq. (2.2) can be written as:

$$G(s) = k\frac{\prod_{zeros}(s^2 + \omega_{0i}^2)}{\prod_{poles}(s^2 + \omega_i^2)} \tag{2.3}$$

where ω_{0i} denotes the i^{th} anti-resonant frequency and ω_i denotes the i^{th} resonant frequency. Figure 2.2 shows the Bode plot for a system described by Eq. (2.3). Each peak is the transfer function magnitude at a resonant frequency described by ω_i and each negative peak is described by ω_{0i}. In this case, the resonance frequencies were selected to be 3, 6, and 10 rad/sec. The anti-resonance frequencies were selected to be 5 and 8 rad/sec. This figure is a typical case of a collocated system because it has an anti-resonant frequency between two consecutive resonant frequencies and the phase oscillates between 0° and 180°.

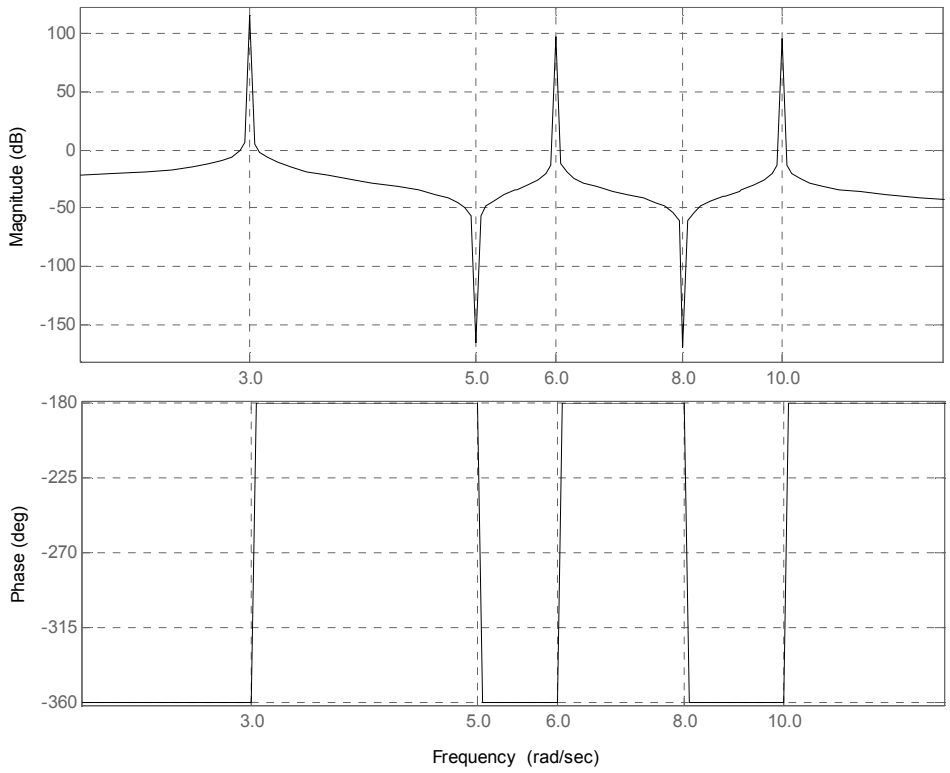

Figure 2.2 Bode plot for a typical collocated system

Figure 2.3 is a typical map of the poles and zeros of an undamped collocated system. In this case, the poles and zeros are located on the imaginary axis. This is a result of a system that is assumed to have no damping. If there was damping, the poles and zeros would be shifted into the left-hand plane.

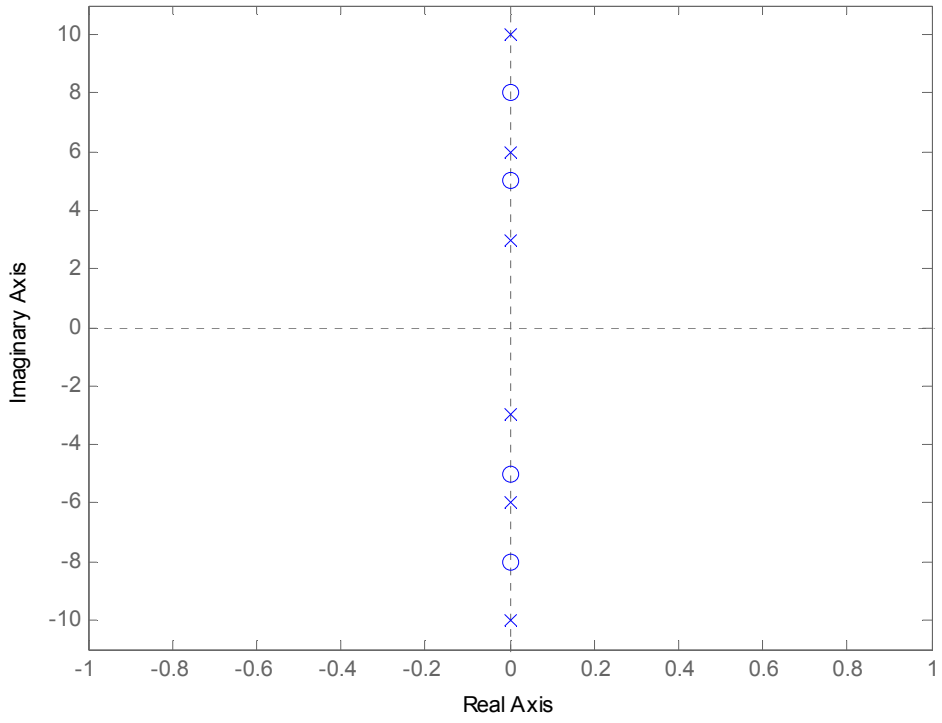

Figure 2.3 Pole-zero map of a typical collocated system without damping

It should be noted that the Figure 2.3 exhibits another unique feature of collocated systems. This unique feature is the property of interlacing poles and zeros. Structures with a collocated actuator and sensor lead to systems with poles and zeros alternating along the imaginary axis [Martin 1978]. Between any two resonant frequencies or poles, resides an anti-resonant frequency, or a zero.

2.3 Examples

2.3.1 Two Mass Collocated System

A two mass system is a simple system that can clearly show the effects of collocation. The system of Fig. 2.4 contains two masses on a frictionless surface. Each

mass is connected to a solid wall by a spring and damper. A third spring and damper are connected between the masses. The displacement of mass one is denoted by q_1 and the displacement of mass two is similarly denoted by q_2. Since this is an actively controlled system, the input force, u, is applied to mass one.

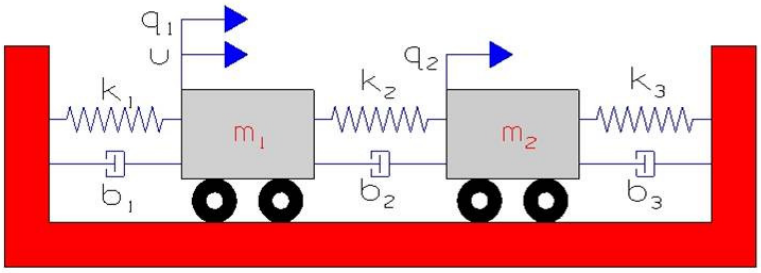

Figure 2.4 Two mass collocated system

In this case, the displacement of mass one, q_1, is controlled at the same point as the input force, u, thus making the system collocated.

A mathematical representation of the system in Fig. 2.4 is derived from the free body diagram of the system. The equations of motion are then found from the application of Newton's Second Law of motion. Once simplified, the system can be described by Eqs. (2.4) and (2.5):

$$m_1\ddot{q}_1 + (b_1 + b_2)\dot{q}_1 + (k_1 + k_2)q_1 = b_2\dot{q}_2 + k_2q_2 + u \tag{2.4}$$

$$m_2\ddot{q}_2 + (b_2 + b_3)\dot{q}_2 + (k_2 + k_3)q_2 = b_2\dot{q}_1 + k_2q_1 \tag{2.5}$$

From here, two approaches can be taken based on Laplace transformation or state space representation. This thesis will follow the Laplace transformation approach which readily leads to a transfer function. Equations (2.4)-(2.5) after applying the Laplace transformation yield:

$$Q_1(s) = \frac{(b_2 s + k_2)Q_2(s) + U}{m_1 s^2 + (b_1 + b_2)s + (k_1 + k_2)} \tag{2.6}$$

$$Q_2(s) = \frac{(b_2 s + k_2)Q_1(s)}{m_2 s^2 + (b_2 + b_3)s + (k_2 + k_3)} \tag{2.7}$$

By substituting Eq. (2.6) into Eq. (2.7), the open loop transfer function, G(s), for the displacement of mass one due to the input force at mass one is found as follows:

$$G(s) = \frac{Q_1(s)}{U(s)} = \frac{(m_2 s^2 + (b_2 + b_3)s + (k_2 + k_3))}{as^4 + bs^3 + cs^2 + ds + e} \tag{2.8}$$

where,

$$\begin{aligned}
a &= m_1 m_2 \\
b &= m_1(b_2 + b_3) + m_2(b_1 + b_2) \\
c &= m_1(k_2 + k_3) + m_2(k_1 + k_2) + b_1(b_2 + b_3) + b_2 b_3 \\
d &= k_1(b_2 + b_3) + k_2(b_1 + b_3) + k_3(b_1 + b_2) \\
e &= k_1(k_2 + k_3) + k_2 k_3
\end{aligned}$$

The roots of the numerator are referred to as the zeros of the system, while the roots of the denominator are considered the poles of the system. Equation (2.8) shows that the system has two zeros and two pairs of poles. Assuming the following parameters:

$m_1 = 10\ kg,\ m_2 = 5\ kg,\ b_1 = 0.05\ \ N - \sec/m,\ b_2 = 0.4\ \ N - \sec/m,\ b_3 = 0.05\ \ N - \sec/m,$

$k_1 = 5\ \ N/m,\ k_2 = 40\ \ N/m,\ k_3 = 5\ \ N/m$ and by employing the use of Matlab software, a root locus diagram shows the placement and the interaction of the poles and zeros. Figure 2.5 presents the root locus plot for the closed loop system where the poles and zeros are denoted as an “x” and as an “o”, respectively. Also, it shows how the poles will move as the feedback gain is increased from 1 to infinity. This plot demonstrates some of the key features of a collocated system. The first feature is the alternating of poles and zeros near the imaginary axis. It should be noted that the poles and zeros are near the

imaginary axis because of the low damping in the system, which is one percent of the stiffness. Another key feature is the stability. Since the stable region is the negative real plane (LH plane), this system is and always will be stable because the poles stay in the negative real plane.

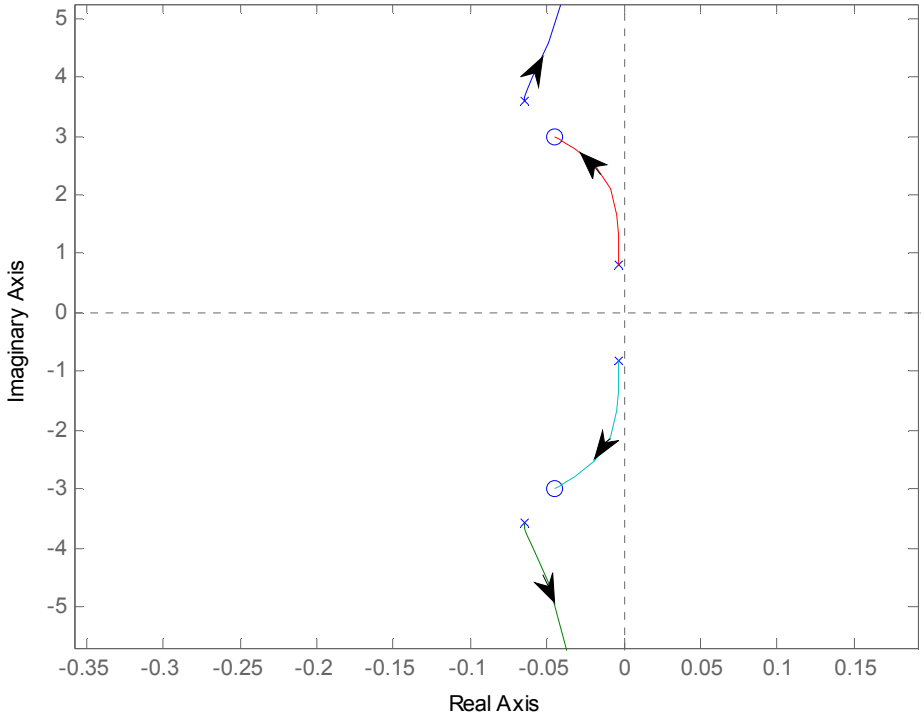

Figure 2.5 Root locus of two-mass collocated system shown in Fig. 2.4

It can be seen that by increasing the gain, the poles follow a locus and finally reach the zeros with which they are paired. The root locus also reveals the damping of each pole along the trajectory, i.e., with the gain increase, the pole initially move away from the imaginary axis and the damping increases until some maximum value. At the position where the pole reaches the zero, the damping is at the maximum value.

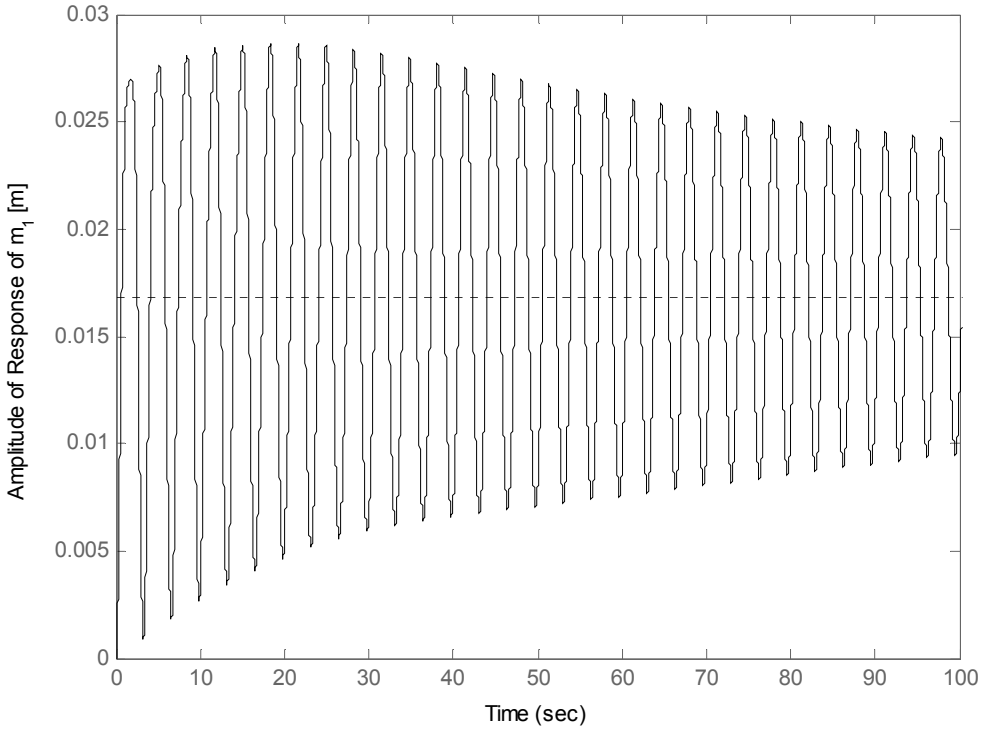

Figure 2.6 Step response of a two mass collocated system with the step input applied to m_1 and measured at m_1

Typically, plotting the step response of a system is useful for understanding the system response characteristics. Figure 2.6 shows the step response of the two mass collocated system. This plot confirms the root locus and further illustrates that this system is stable because the amplitude of the response converges to a certain steady-state value. In this case, the response converges to 0.168 m in approximately 1000 seconds. The time is long due to the low damping in the system.

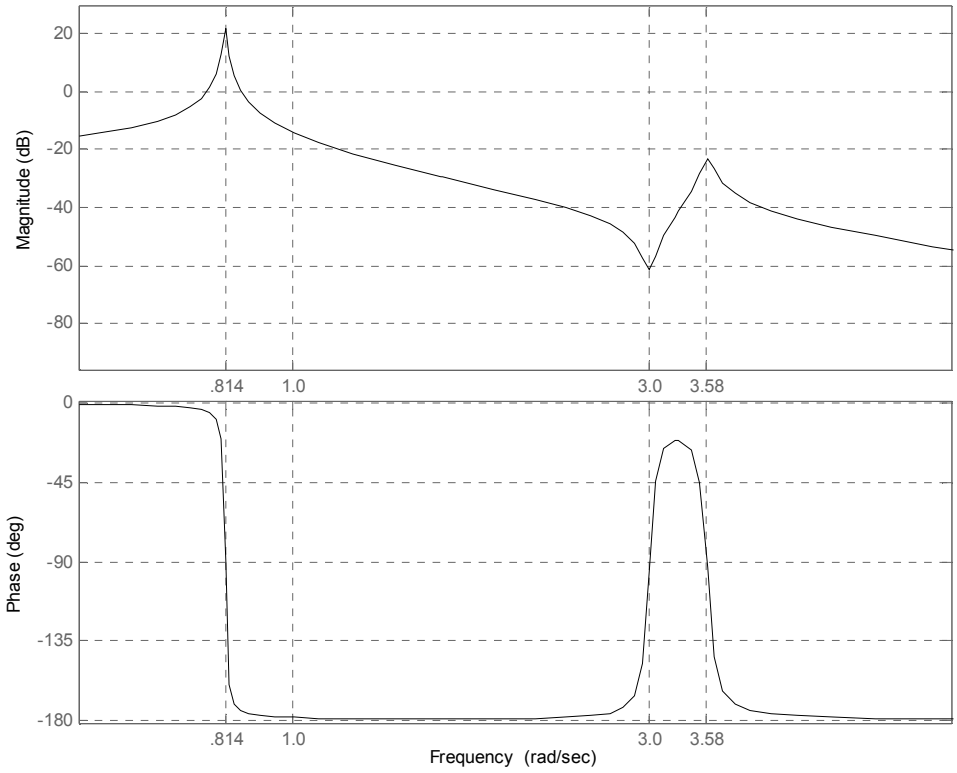

Figure 2.7 Bode plot of two-mass collocated system shown in Fig. 2.4

Further analysis demonstrates the characteristics of a collocated system through Bode plots, Fig. 2.7. The Bode plots shows the magnitude and phase of the transfer function, Eq. (2.8). Since this is a two mass system with two degrees of freedom, there are two peaks in amplitude which represent the natural or resonance frequencies. A feature of collocated systems is the presence of an anti-resonant frequency between two consecutive resonance frequencies. A harmonic excitation at an anti-resonance frequency produces no response at the degree of freedom where the excitation is applied. The structure will have the same response as a structure that has an additional restraint at the location of the collocated sensor and actuator. Furthermore, the zeros of the

collocated system are in fact the natural frequencies of the same system with the additional restraint at the collocated sensor and actuator [Miu 1991]. In the case of the system in Fig. 2.4, this is proven to be true. If an additional restraint is added to m_1, the equation of motion yield:

$$m_2\ddot{q}_2 + (b_2 + b_3)\dot{q}_2 + (k_2 + k_3)q_2 = 0 \tag{2.9}$$

Applying the Laplace transform, Eq. (2.9) becomes:

$$[m_2 s^2 + (b_2 + b_3)s + (k_2 + k_3)]Q_2(s) = 0 \tag{2.10}$$

The roots of the above equation are the natural frequencies. These roots are identical to the numerator of Eq. (2.8), which are the zeros of the entire system.

It should be noted that anti-resonant frequencies are based on sensor and actuator locations. Resonant frequencies are based on the dynamics of the system and are not influenced by the position of the sensors and actuators. Between two consecutive resonant frequencies, only one anti-resonant frequency can exist. This is due to the feature of alternating poles and zeros, commonly known as interlacing.

The Bode diagram of Fig. 2.7 shows a 180° phase lag at every resonant frequency and a 180° phase lead at every anti-resonant frequency. This is a characteristic of collocated systems.

2.3.2 Two Mass Non-collocated System

The previous section described a collocated system as a system that placed a sensor at the same location as the input force. Therefore, a non-collocated system is a system where the sensor is not placed at the location of the input force. As it was discussed, a collocated system has alternating poles and zeros which makes the system

stable. However, in a non-collocated system this is not the case. This type of system is not preferred, but in some cases required. One such example is a system with active magnetic bearings [Sawicki 2007].

Consider the system shown in Fig. 2.8. This system is the same as the system shown in Fig. 2.4, but the input force is acting on mass two. The displacement of mass one is denoted by q_1 and the displacement of mass two is denoted by q_2. Since this is an actively controlled system, the input force, u, is applied to mass two.

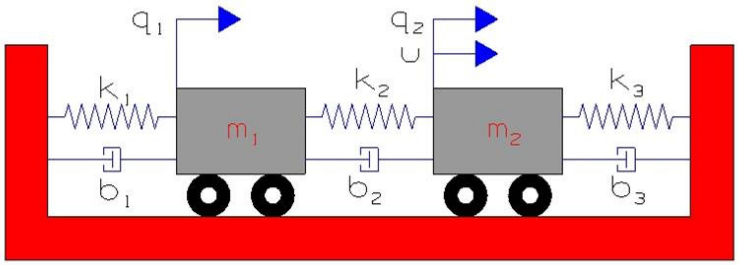

Figure 2.8 Two-mass non-collocated system

In this case, the displacement of mass one is measured at a different point than the input force. This makes the system so called non-collocated.

A mathematical representation of the system shown in Fig. 2.8 is derived from the free body diagram of the system. As with the system shown in Fig. 2.4, the equations of motion are then found from the application of Newton's Second Law of motion. Once simplified, the system can be described by:

$$m_1\ddot{q}_1 + (b_1 + b_2)\dot{q}_1 + (k_1 + k_2)q_1 = b_2\dot{q}_2 + k_2 q_2 \tag{2.11}$$

$$m_2\ddot{q}_2 + (b_2 + b_3)\dot{q}_2 + (k_2 + k_3)q_2 = b_2\dot{q}_1 + k_2 q_1 + u \tag{2.12}$$

After the application of Laplace transformations, Eqs. (2.11) and (2.12) become Eqs. (2.13) and (2.14).

$$Q_1(s) = \frac{(b_2 s + k_2)Q_2(s)}{m_1 s^2 + (b_1 + b_2)s + (k_1 + k_2)} \tag{2.13}$$

$$Q_2(s) = \frac{(b_2 s + k_2)Q_1(s) + U}{m_2 s^2 + (b_2 + b_3)s + (k_2 + k_3)} \tag{2.14}$$

By substituting Eq. (2.13) into Eq. (2.14), the open loop transfer function, G(s), for the displacement of mass one to the input force is found to be:

$$G(s) = \frac{Q_1(s)}{U(s)} = \frac{b_2 s + k_2}{as^4 + bs^3 + cs^2 + ds + e} \tag{2.15}$$

The coefficients of the denominator are the same as Eq. (2.8). Equation (2.15) has the same denominator as Eq. (2.8); however, the numerator has one root at $-k_2/b_2$. This is true because the poles of any system do not depend on the sensor location. Intuitively, this is accurate because the natural frequencies of a system are based on the mass and stiffness and not sensor and actuator locations.

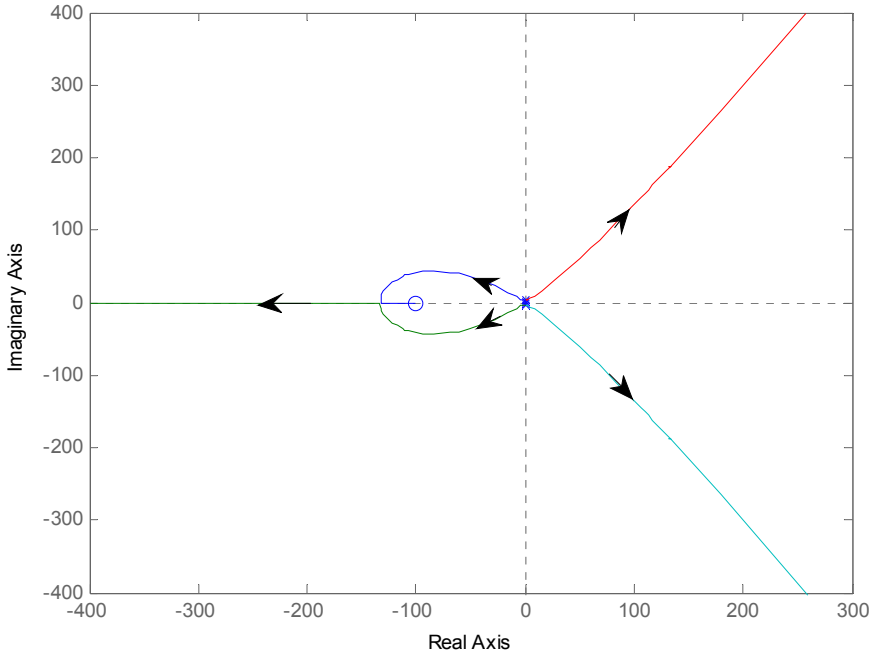

Figure 2.9 Root Locus of two-mass non-collocated system shown in Fig. 2.8

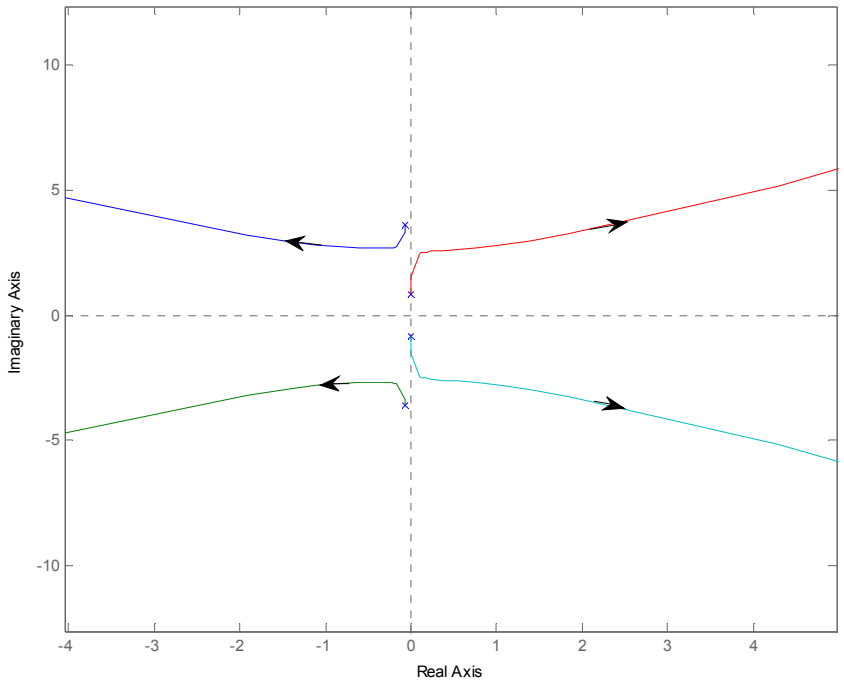

Figure 2.10 Close up of root locus for two-mass non-collocated system shown in Fig. 2.8

Figures 2.9 and 2.10 show the root locus plots for this system. Figure 2.9 shows the zero location along the real axis and Fig. 2.10 shows the poles near the imaginary axis. This plot is significantly different than the plot of the collocated root locus. In the case of the collocated root locus, there are alternating poles and zeros due to the presence of imaginary zeros. Those same imaginary zeros are no longer present; therefore, the system can very quickly become unstable as the poles travel into the positive RH plane.

The step response of this system is very different than of the previous collocated system. Figure 2.10 suggests that a small gain will cause the system to become unstable.

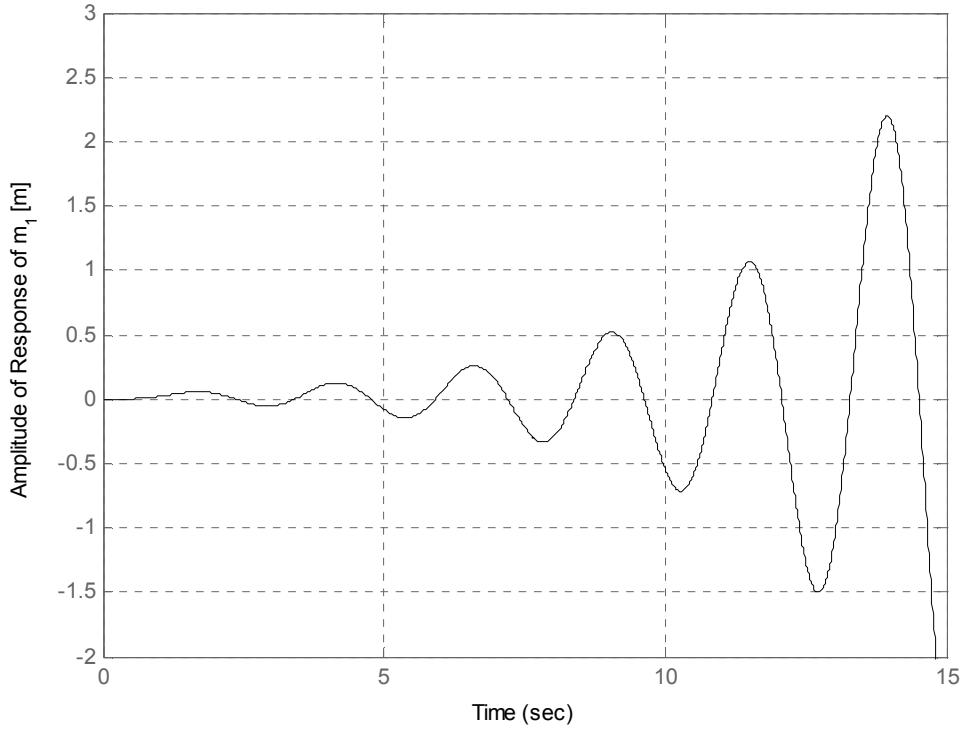

Figure 2.11 Step response of a two-mass non-collocated system with a gain of 50 and step input applied to m_2 and measured at m_1

This is confirmed in Fig. 2.11 which illustrates the step response with a gain of 50. In this case, the step input is applied to m_2 and the response of m_1 is shown above. Here the response begins at zero, and then the response starts to increase exponentially. Stable systems will show the amplitude of the response converge to a certain value; however, in unstable systems, the amplitude of the response increases to infinity.

Figure 2.12 shows the Bode plots and the absence of the anti-resonance between the same two resonant frequencies. While there is still the 180° phase lag from each of the resonant frequencies, there is no anti-resonant frequency and therefore there is no 180° phase lead. This has the effect of the second resonance having a phase of -270° while the collocated counterpart possesses a phase of -90°.

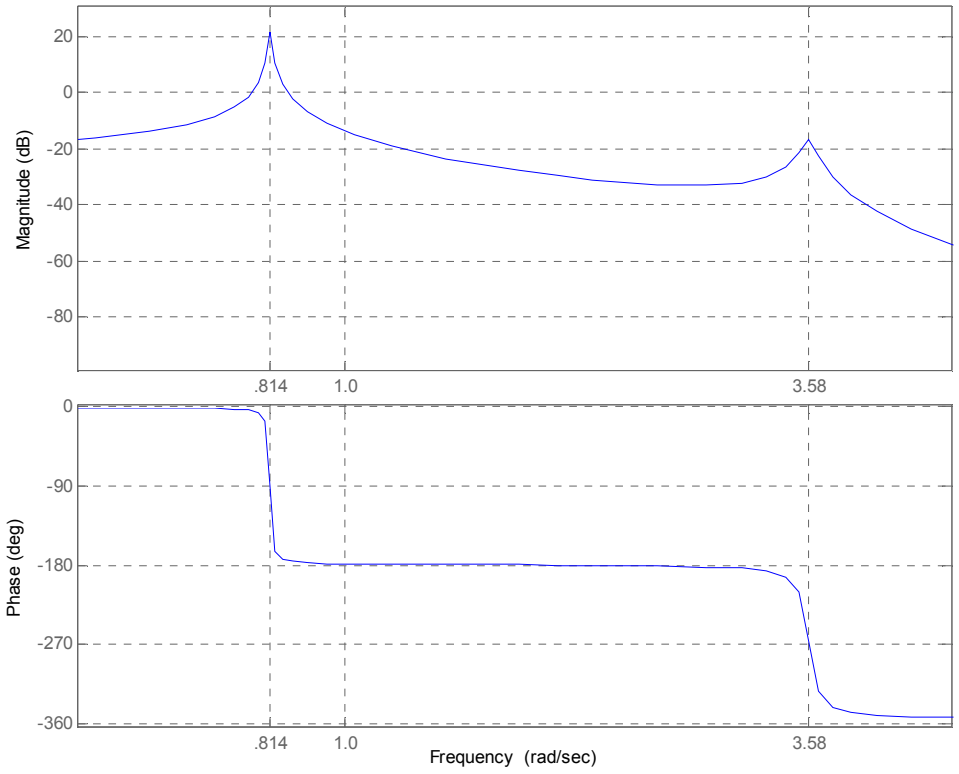

Figure 2.12 Bode plot of two-mass non-collocated system shown in Fig. 2.8

2.3.3 Flexible Beam

The effects of non-collocation are not limited to simple two mass systems. The same effects can be seen on more complicated structures, i.e., a flexible beam. Figure 2.13 shows the geometry of a flexible beam. This shows a pinned condition at 10 m from the left end of the beam. The arrow represents the actuating force and it is located at 45 m from the left end. The small cylinders on either side of the arrow indicate the non-collocated sensor locations. Table I shows the properties of the beam.

Length (m)	60
Outside Diameter (m)	1
Inside Diameter (m)	0
Density (kg/m^3)	7850
Young's Modulus (GPa)	210
Pinned Location (m)	10
Actuator Location (m)	45

Table I Properties of the flexible beam

Nine sensor locations are going to be investigated. The first location is at the actuator to represent the collocated case and then moved to the right and to the left in one meter increments up to five meters. Matlab along with an FEA program will be used to perform the analysis.

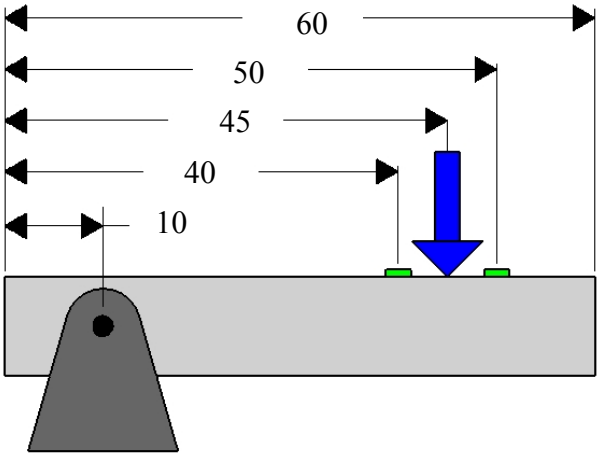

Figure 2.13 Flexible beam geometry, dimensions in m

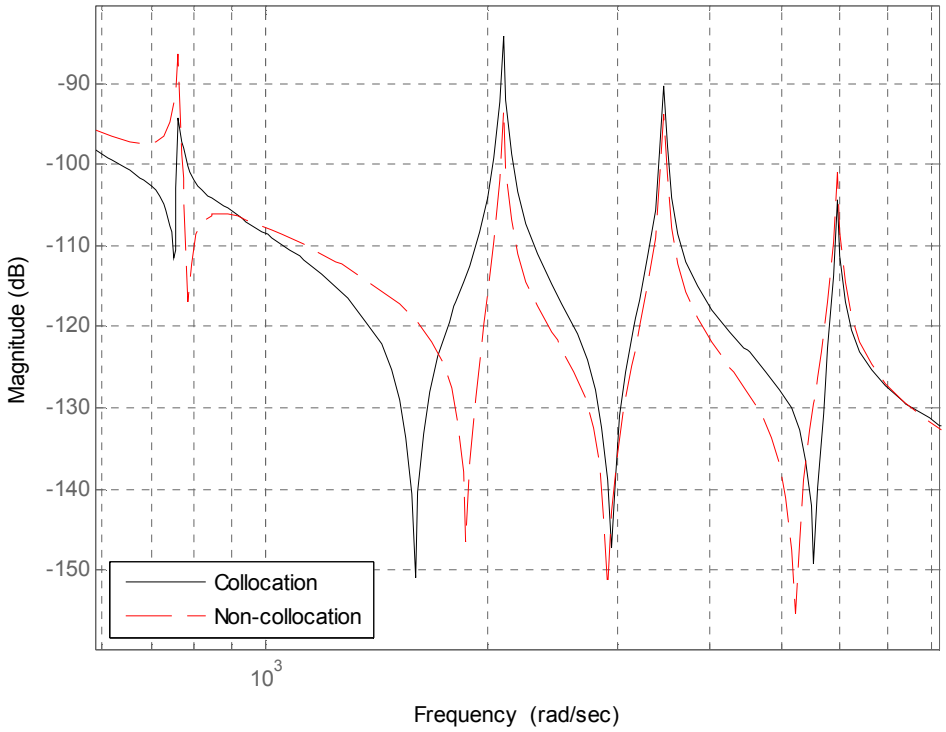

Figure 2.14 Bode plot of flexible beam at collocated and RH non-collocated locations

Figure 2.14 shows the Bode plot for the collocated sensor location and the non-collocated location of 5 m to the right of the actuator. It is important to note that the peaks of the

plot are in the identical place. The peaks represent the natural frequencies of the system and there are four of them within the frequency range being analyzed, at frequencies 763, 2100, 3460, and 5960 rad/sec This will always occur because only the sensor location was changed; therefore, the natural frequencies of the system were not altered. However, the anti-resonances, or zeros, are altered. Furthermore, each zero is affected in a different manner. The first two zeros are shifted to the right, the third is essentially in the same place and the fourth is shifted to the left. The first zero is on the left side of the first pole in the collocated case and is to the right of the pole in the non-collocated case. This is due to the mode shapes, as shown in Fig. 2.15. The node of the first mode lies between the sensor and actuator. The node of a mode shape is the point at which there is zero response for a given input. Therefore, as the sensor moves towards the non-collocated location, the zero jumps over the pole and moves to a higher frequency. The point at which the zero moves to a higher frequency than the pole, is the point at which the property of pole-zero interlacing is lost. This is shown in Fig. 2.17. The same phenomenon is occurring to the second zero except in this case, the node of the second mode is just beyond the non-collocated case. If the sensor would be moved an additional 2 m, this zero would move to the other side of the pole as well. The third zero doesn't move very much and this is due to no nodes being near the third pole. The fourth zero is moving in the opposite direction. This seems to be incorrect, but again, it is a function of the mode shapes. In this case, the node of the fourth mode lies just to the left of the fourth pole. Therefore, the non-collocated case is actually farther away from the node than the collocated case. This results in a lower frequency. This concept will become clearer later in this section when the sensor is moved to the left of the actuator.

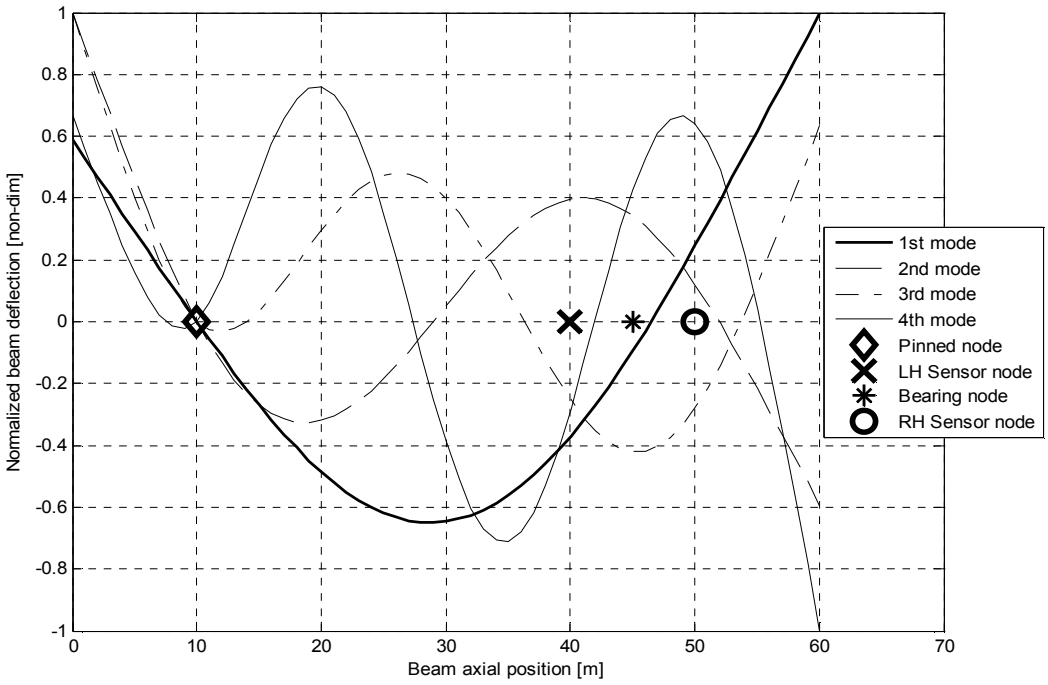

Figure 2.15 Mode shapes of the flexible beam

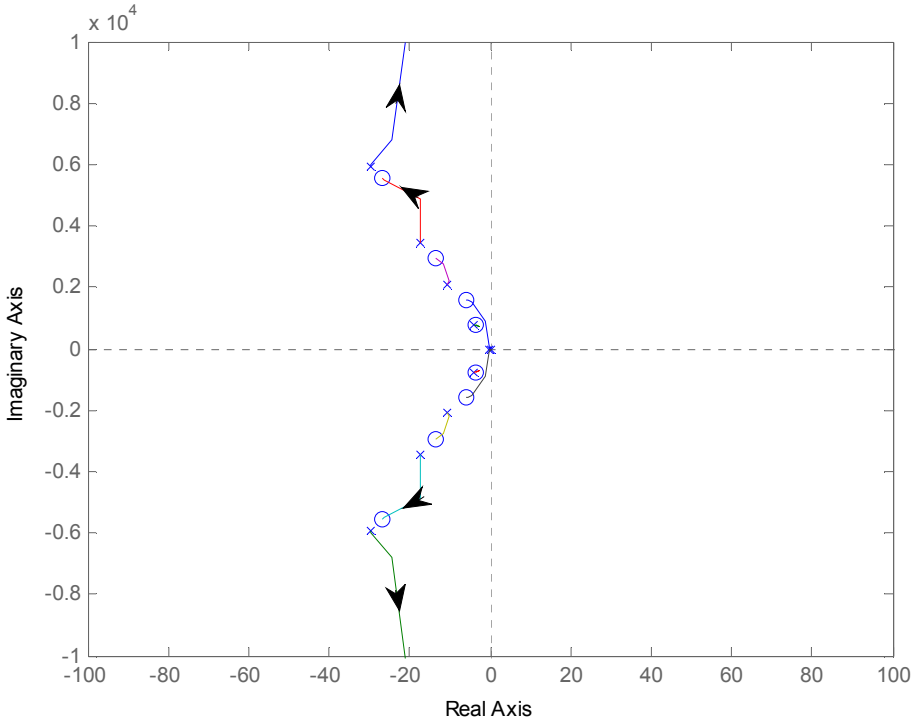

Figure 2.16 Root locus of collocated flexible beam with 0.5% damping

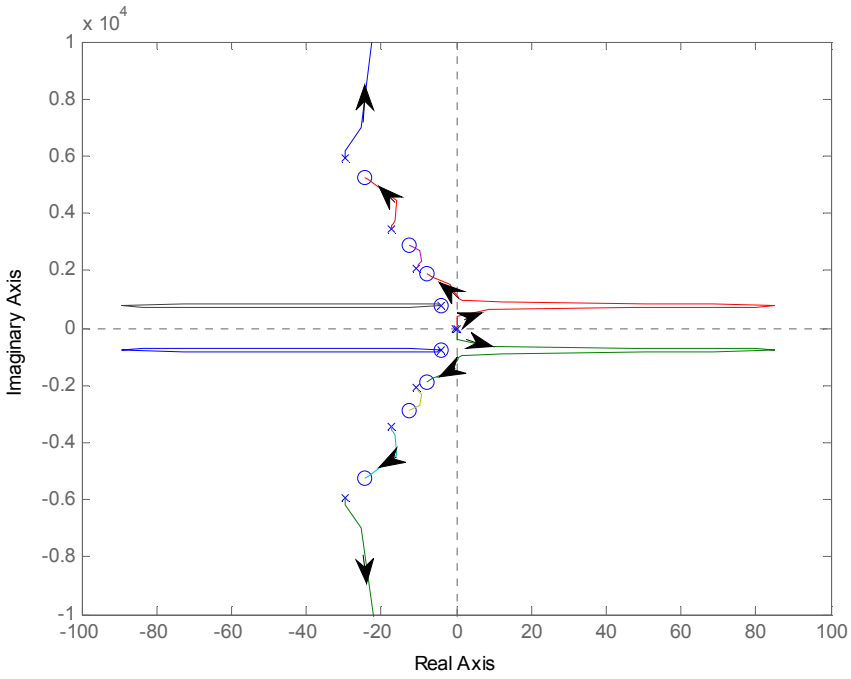

Figure 2.17 Root locus of non-collocated flexible beam with sensor moved 5 m to the right

Figure 2.16 shows the root locus plot of the collocated case while Fig. 2.17 shows the root locus of the non-collocated case where the sensor is moved five meters away from the actuating force. These two plots agree with the Bode plot. Since the poles are the natural frequencies of the system, the root locus shows them unchanged. Another thing to notice on the root locus plots is the phenomenon of alternating poles and zeros. This occurs in the collocated case but does not occur in the non-collocated case. As a result, the collocated system is much more stable than the non-collocated system. This is shown in the non-collocated root locus diagram. The reason the poles of Fig. 2.17 travel into the unstable region is because the first zero moves to a higher frequency than the first non-zero pole. Therefore, the pole at zero must travel around the first pole-zero pair to

cancel with the second zero. When the poles travel to the right hand plane, the system becomes unstable and uncontrollable. This does not occur in the collocated system.

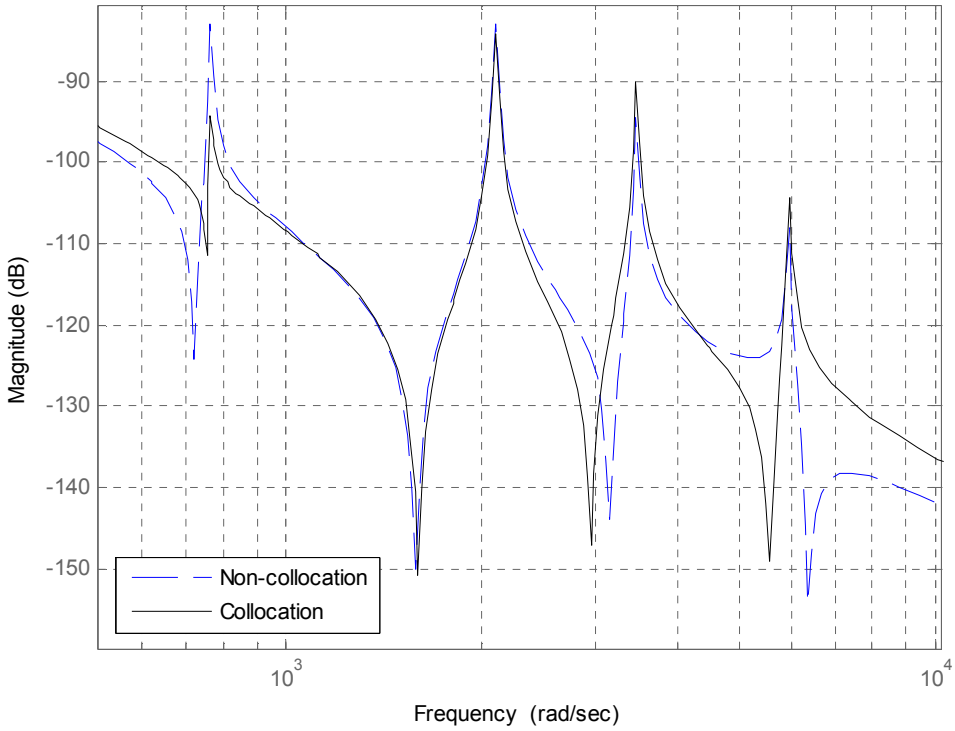

Figure 2.18 Bode plot of flexible beam at collocated and LH non-collocated locations

The same analysis was performed when the sensor was moved in one meter increments to the left of the actuating force up to five meters. Very similar results can be seen, with the exception of the effects on different anti-resonances. This can be seen in Fig. 2.18. In this case, the first zero is shifted to the left, the second zero is nearly unchanged and the third and fourth zeros are shifted to the right. All these results are to be expected. The first zero is shifted to the left because it is moving farther away from the node of the first mode. The second zero is nearly unchanged because there is node near the second pole. The third zero is shifted to the right because it is approaching a

node which is only 4 m farther away. The fourth zero moved from the left side of the fourth pole to the right side. This is due to the node of the fourth mode lying between the actuator and non-collocated sensor. In this non-collocated case, the property of pole-zero interlacing is lost because the fourth zero is no longer between the third and fourth poles.

The root locus plots for the collocated case and the non-collocated case are shown in Figs. 2.19 and 2.20. These appear different than the previous case, and this is due to damping. The previous case had 0.5% damping added to the system and this case does not have any damping. As with the previous case, the collocated system is stable because the poles do not travel into the right hand plane. However, the non-collocated system can quickly become unstable due to the poles entering the right hand plane. The collocated case shows the phenomenon of alternating poles and zeros, while the non-collocated case demonstrates the phenomenon of pole-zero flipping. The reason why the collocated case is stable while the non-collocated case is not, is due to the flipping of the fourth non-zero pole and fourth zero of the non-collocated case. This causes the fourth pole to travel into the right hand plane to avoid the fifth pole on its way to infinity. Pole-zero flipping occurs when the zero coincides with a node of a particular mode [Preumont 2002]. In this case, a zero coincides with the fourth flexible mode.

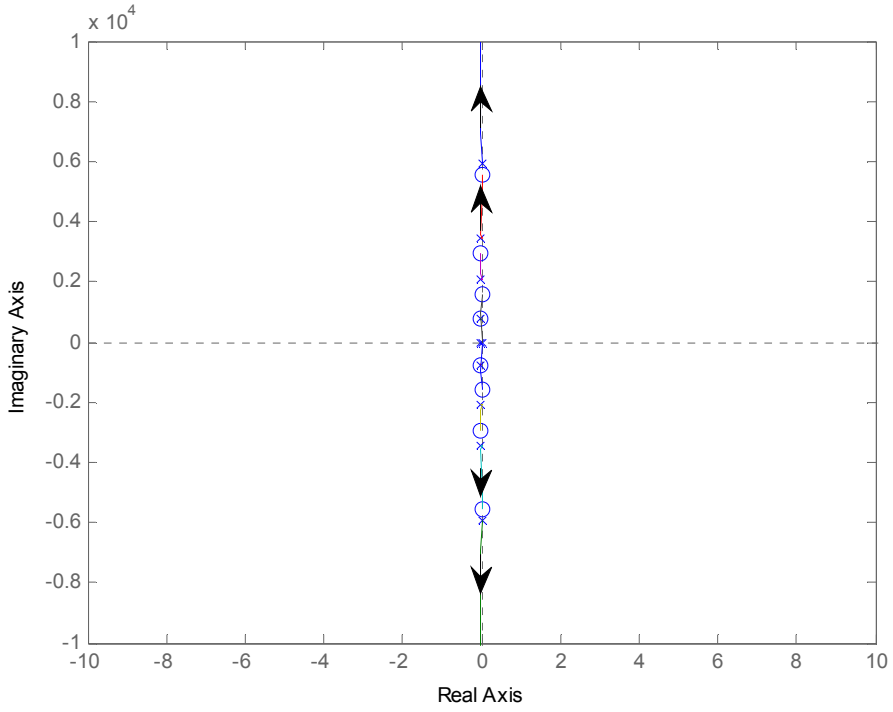

Figure 2.19 Root locus of collocated flexible beam with no damping

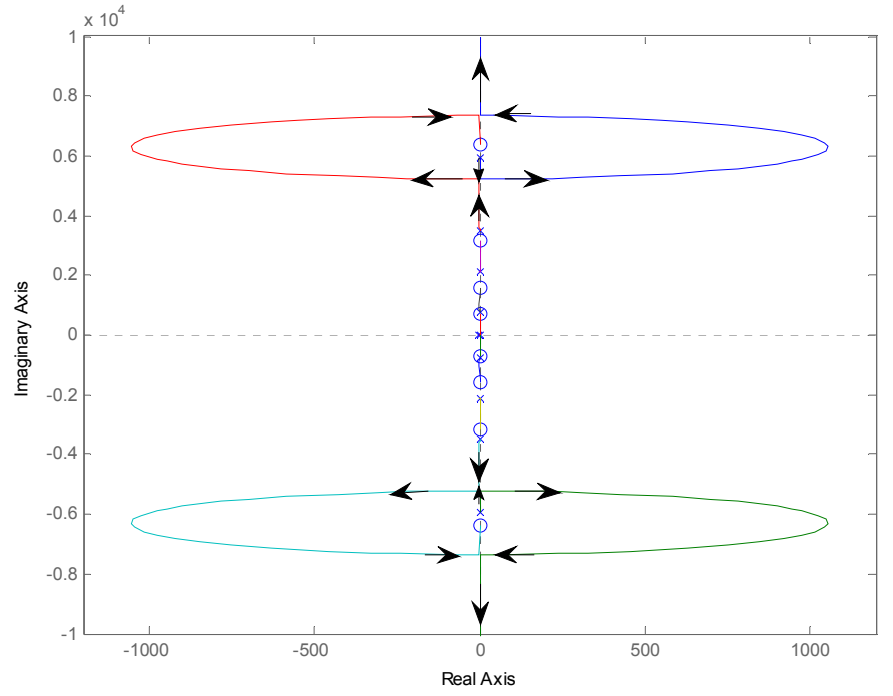

Figure 2.20 Root locus of non-collocated flexible beam with no damping

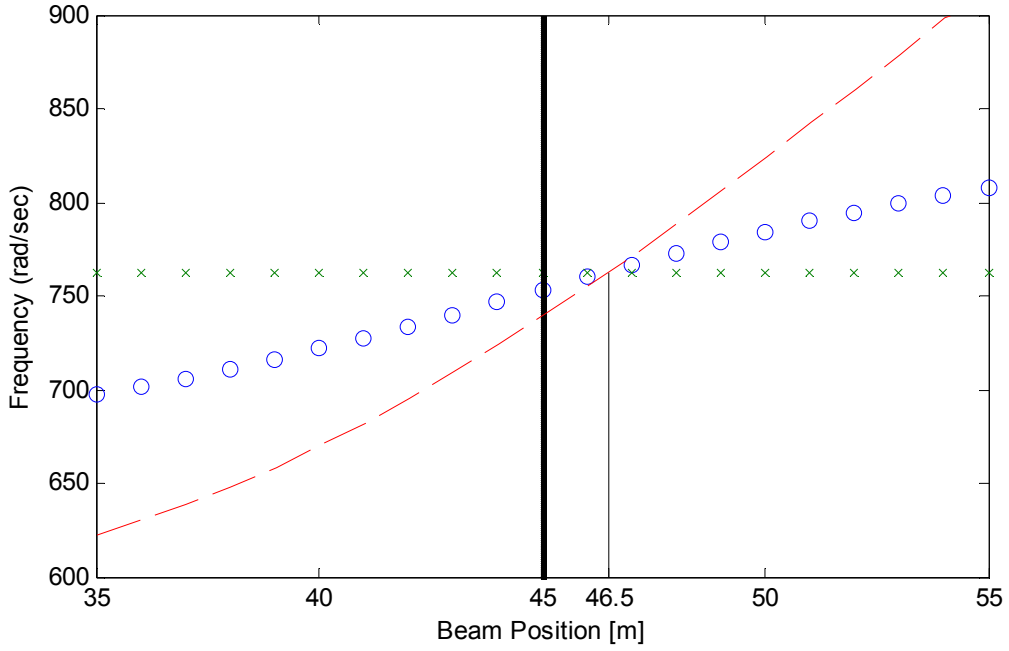

Figure 2.21 Zeros of the flexible beam as a function of the sensor location at the first mode

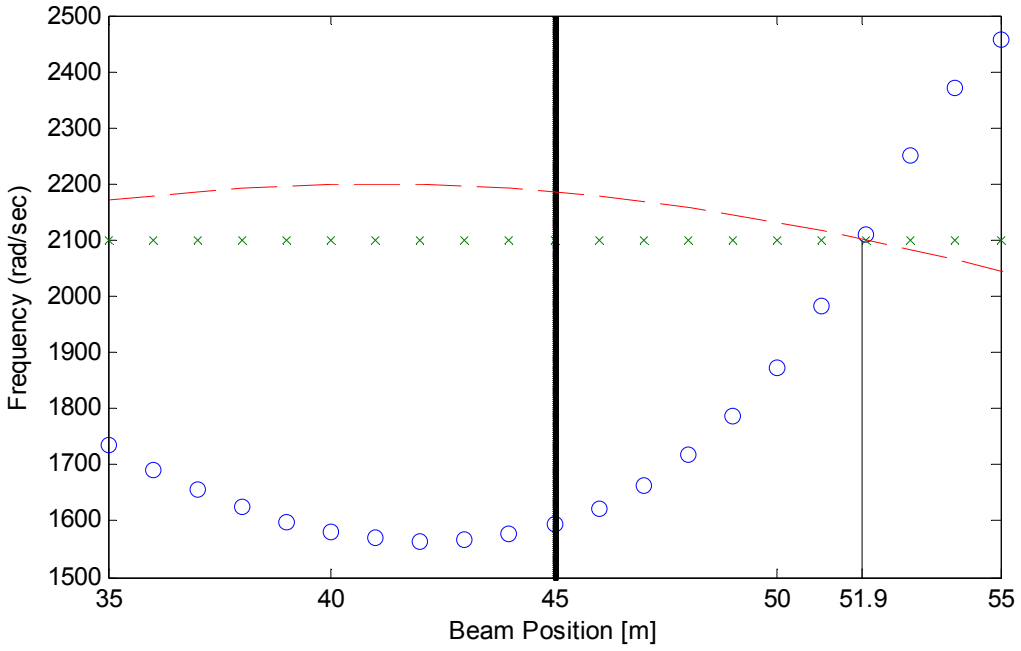

Figure 2.22 Zeros of the flexible beam as a function of the sensor location at the second mode

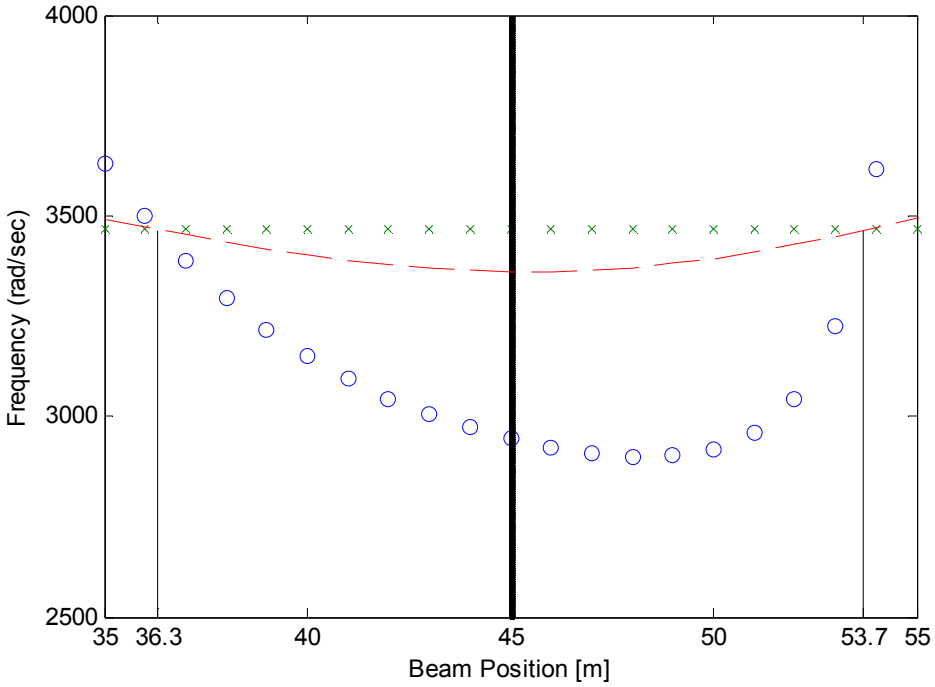

Figure 2.23 Zeros of the flexible beam as a function of the sensor location at the third mode

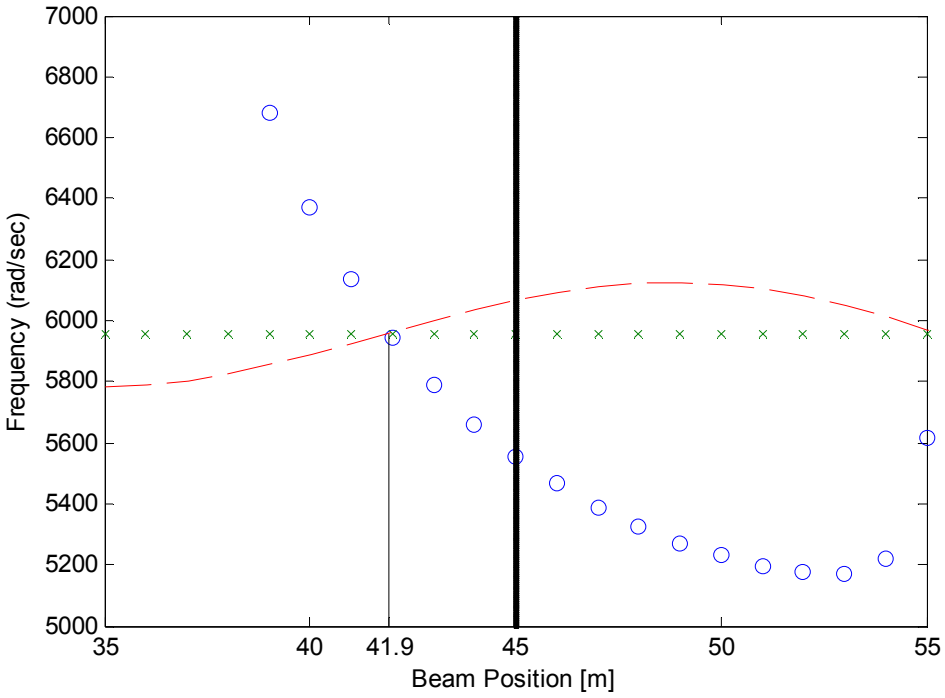

Figure 2.24 Zeros of the flexible beam as a function of the sensor location at the fourth mode

Figures 2.21 - 2.24 shows the frequency of the zeros as a function of sensor position. In this case, the actuator is kept at the same location shown in Fig. 2.13, 45 m from the left end. The sensor is initially located at 35 m from the left end and is moved in 1 m increments up to 55 m. The first four flexible mode shapes are displayed along with the frequency of the poles. As it is shown, the poles, shown as an 'x', are at the same frequency regardless of the sensor position; however, the zeros, shown as a 'o', are not. At 45 m, the sensor is at the same location as the actuator; therefore, it is the collocated case. At this location there is pole-zero interlacing. This figure also shows vertical lines. These correspond to the nodes of the various mode shapes.

	Natural Frequency (rad/sec)	Node 1 (m)	Node 2 (m)	Node 3 (m)	Node 4 (m)	Node 5 (m)
Mode 1	762.7	10	46.5	-	-	-
Mode 2	2100.5	10	29	51.9	-	-
Mode 3	3464.3	10	13.9	36.3	53.7	-
Mode 4	5959.4	7.6	10	27	41.9	55.3

Table II Axial positions of each node for each mode

Table II lists all the axial positions of the nodes of each mode shape. At each node, the mode shape and zeros cross the frequency of the poles. This is a problem because the property of pole-zero interlacing vanishes, and this leads to instability. Figure 2.25 demonstrates this phenomenon by showing the poles and zeros of the collocated system on the left, and the non-collocated system on the right. The non-collocated plot shows the system when the sensor is placed at node 52. This location is 1

m beyond the node of the second mode shape. In this case, there is pole-zero flipping because the order of the pole and zero is 'flipped'. The first pole of the collocated system can travel along the imaginary axis to cancel with the second zero; however, in the non-collocated case, the first pole must travel around the second pole and into the unstable region to cancel with the second zero.

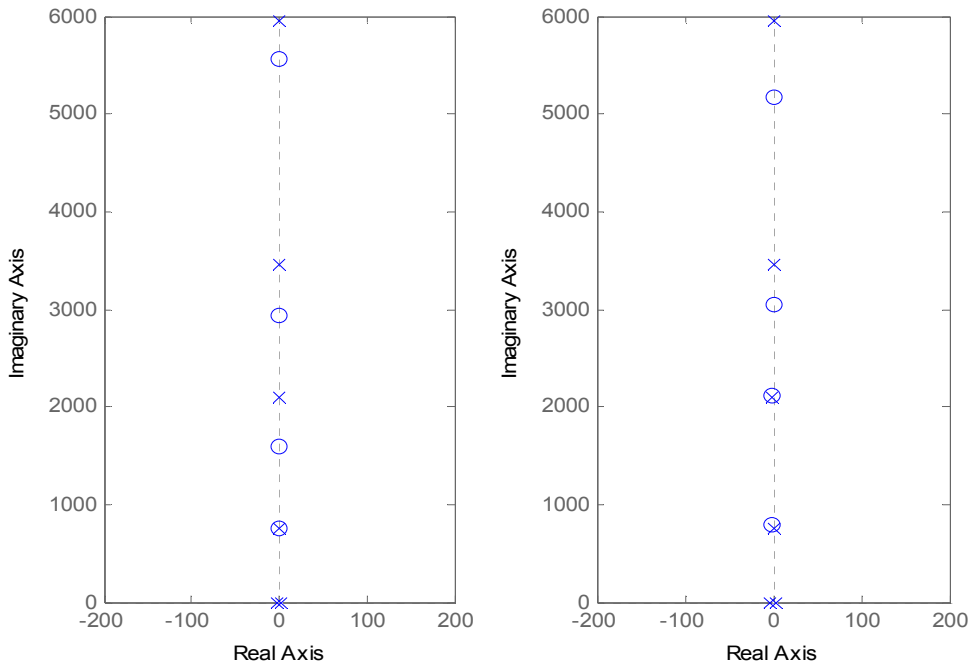

Figure 2.25 Pole-zero map of the flexible beam, collocated on left and non-collocated on right

2.3.4 Experimental Modal Analysis of Rotor

The previous examples were based on mathematical models which may represent real life systems. This example compares a finite element model of a known rotor with experimental data.

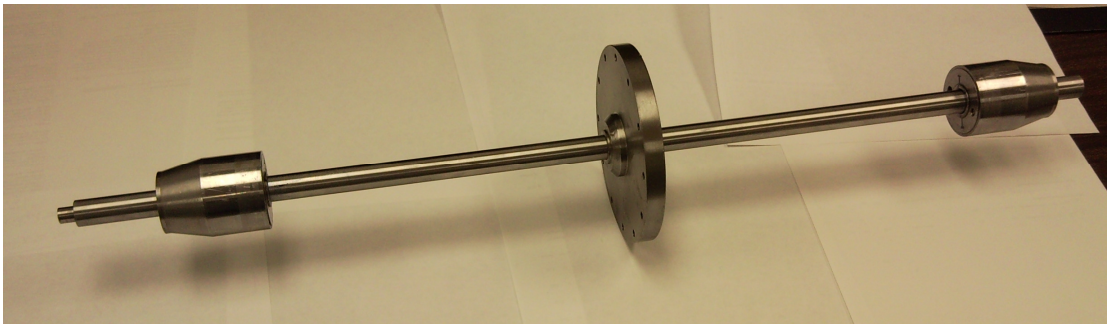

Figure 2.26 Rotor with single disc and conical magnetic bearing rotors

Figure 2.26 is a picture of the rotor that will be used in the analysis. The calculations were done with finite element software. This rotor was sliced into 51 finite elements which results into 52 nodes. Figure 2.27 shows the finite element model and locations of the bearings, sensor, and where both impulses are applied. One impulse is applied at node 17. This is close to the sensor; thus, replicating a collocated case. The second impulse is applied at node 34. This is far enough away from the sensor at node 15 to replicate a non-collocated case.

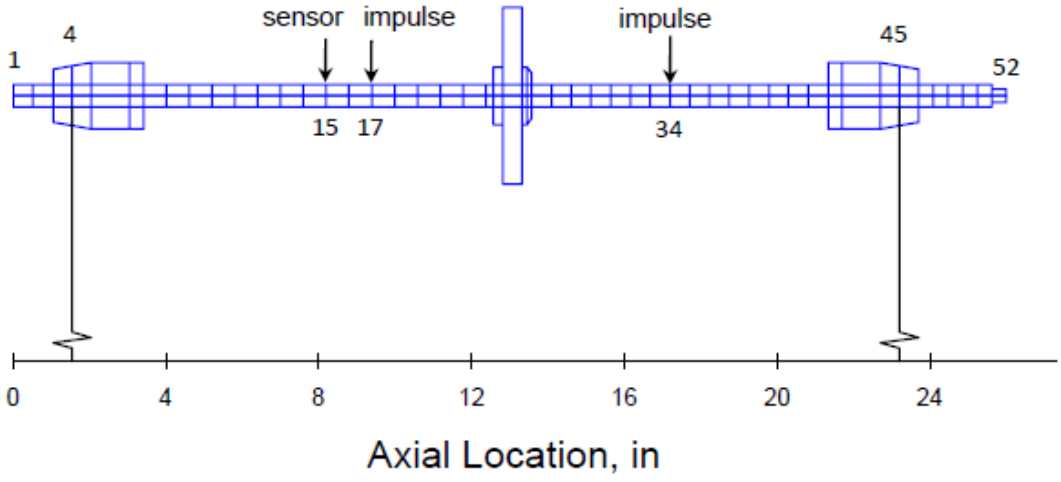

Figure 2.27 Finite element model of rotor shown in Fig. 2.26 and locations of bearings, sensor, and two impulses

The reason for the experiment is to study the effects of collocation versus non-collocation and to replicate the modeling results returned by the FEA software. The FEA software assumes the rotor to be free-free. This simply means that the rotor is not constrained by bearings or anything else. Essentially this means that it is floating in space. This is replicated by supporting the rotor with two thin wires at nodes 4 and 45. The effects of the wires are small, but they do contribute to deviations from the FEA software.

Three experimental trials were performed. Two of the three trials were done for the collocated case to ensure accuracy and the third trial examined the non-collocated case. These results were then plotted against the theoretical results returned by the FEA software.

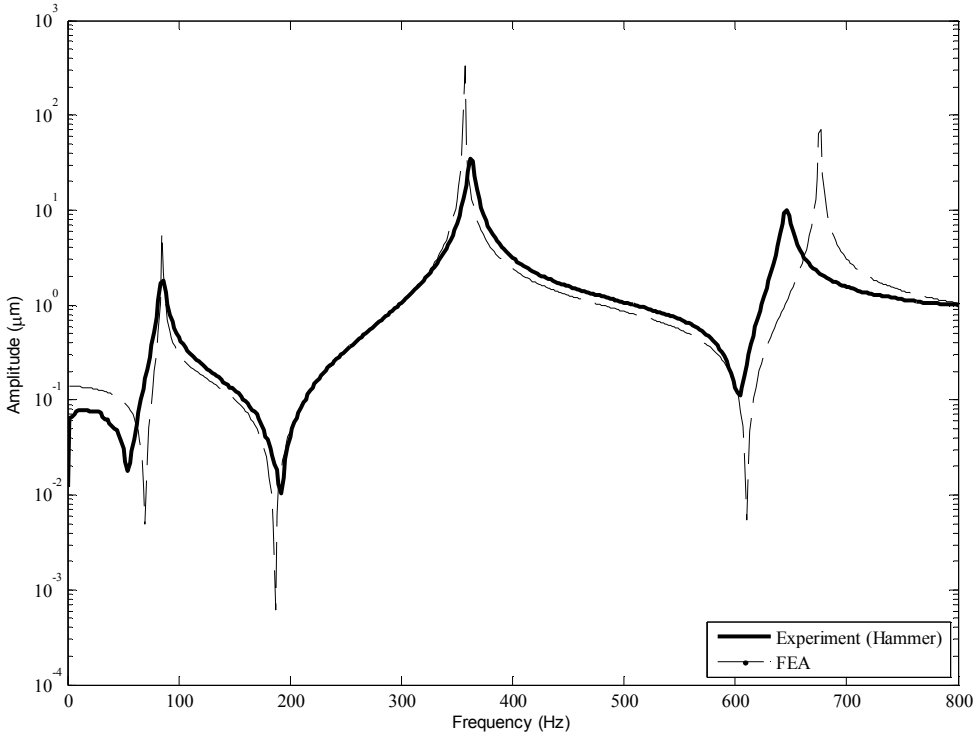

Figure 2.28 Experimental and FEA frequency response

Figure 2.28 shows the results of the experimental collocated case plotted against the theoretical collocated case. The experimental data is a close match for the first and second natural frequencies, while the third natural frequency is approximately 50 Hz less than the theoretical. There can be many explanations why this difference exists. The largest contributions would be inaccuracies between the physical part and the mathematical model. Very rarely will a mathematical model be a one hundred percent match for the physical part. In this case, the conical magnetic bearing rotors are pressed onto the main rotor. This is difficult to accurately model in FEA software. Also, the physical part has twelve 0.05 inch holes in the disc, and this is not accounted for in the FEA software. A second point lies in the experiment itself. The experiment required the use of wires to hold the part in place, while the FEA software assumed a free-free rotor. Finally, a third reason for inaccuracies would be in measuring the output signal. The instrumentation is more sensitive to higher frequencies, which makes errors more likely.

The anti-resonances are also a close match between the experimental and the theoretical. The slight differences are explained by Fig. 2.27. The sensor is at node 15 while the impulse was applied at node 17. Since the difference is small, the anti-resonances are only slightly shifted.

Overall, the experimental data is very repeatable which is demonstrated by Fig. 2.29. Three experiments were done. Two of the three were done for the collocated case to ensure accuracy while the third represented the non-collocated case. It is hard to see all three plots because for the most part, the lines are on top of each other. Regardless of the where the impulse was applied, all three correctly show the same natural frequencies.

As expected, the second and third anti-resonances disappear while the first is shifted. Figure 2.29 also shows the coherence for the three experiments. Coherence is a non-dimensional value that is used to compare the various trials experiments. When the coherence has a value of one, there is no variation between the trials. The coherence is equal to one for most of the frequency range. This implies the data is repeatable and the results are valid. However, the coherence varies at the anti-resonances. These variations are a direct result of the absence of the anti-resonances in the non-collocated experiment. In this case, the data from the collocated experiments is being compared to the data from the non-collocated experiment and this results in the coherence variations.

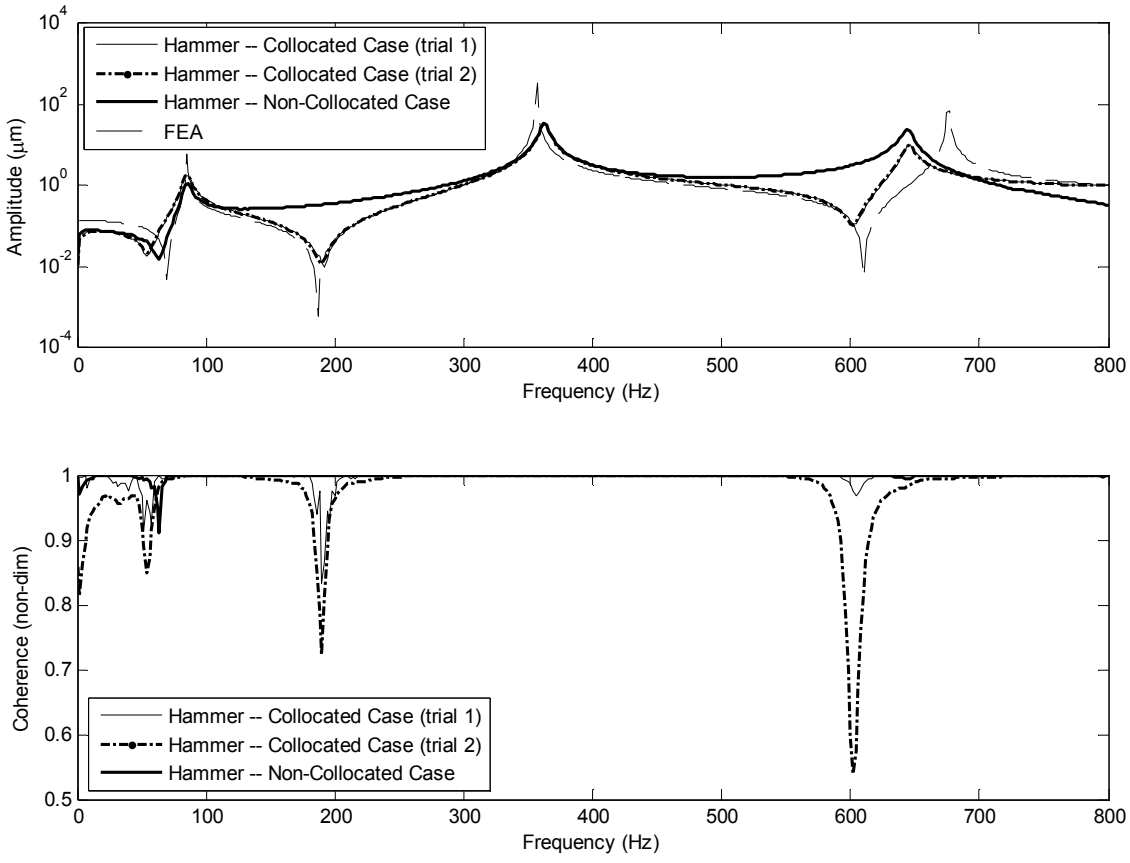

Figure 2.29 Complete frequency response of the impulse test

2.4 Conclusions

Collocated systems enjoy unique characteristics that inherently allow for greater stability. This is a result of alternating poles and zeros. When the poles and zeros are alternating, they will cancel each other. When poles and zeros do not alternate, as in the case of non-collocated systems, the poles can travel into the RH plane of the real and imaginary coordinate system. This was demonstrated in a number of examples. Overall, a collocated system will exhibit the same behavior as a system with an additional restraint at the location of the collocated sensor and actuator.

It is important to note, that the system poles are not dependent on sensor location. However, the system zeros are completely dependent on the location of the sensor relative to the actuator. The amount of influence of the sensor location is dependent on the mode shapes of the system. The flexible beam example examined the effect when a sensor crosses a node of a mode shape. It resulted in the disappearance of the anti-resonance frequency due to pole-zero flipping. The root cause of all of the phenomenon associated with collocation versus non-collocation can be traced back to deflection. In the case of collocation, the sensor is measuring the exact deflection at the actuator. In the case of non-collocation, the sensor is measuring a deflection and it is different than the deflection at the actuator. The mode shapes of the system will predict what the difference is and direction of the deflection, positive or negative. The most unstable scenario occurs when the sensor crosses a node of the mode shape. When this occurs, the sensor is reading zero deflection while there actually is a deflection at the support or actuator. The control system designer of a non-collocated system must be aware and take into account this scenario or the system will not behave as intended and become unstable [Buhr 1997].

CHAPTER III

MODIFIED JEFFCOTT ROTOR ON AMB'S

3.1 Introduction

The Jeffcott rotor is a simple but powerful model in the understanding of rotordynamics. The standard Jeffcott rotor consists of a massive unbalanced disc mounted between rigid supports on a flexible shaft of negligible mass [Vance 1988].

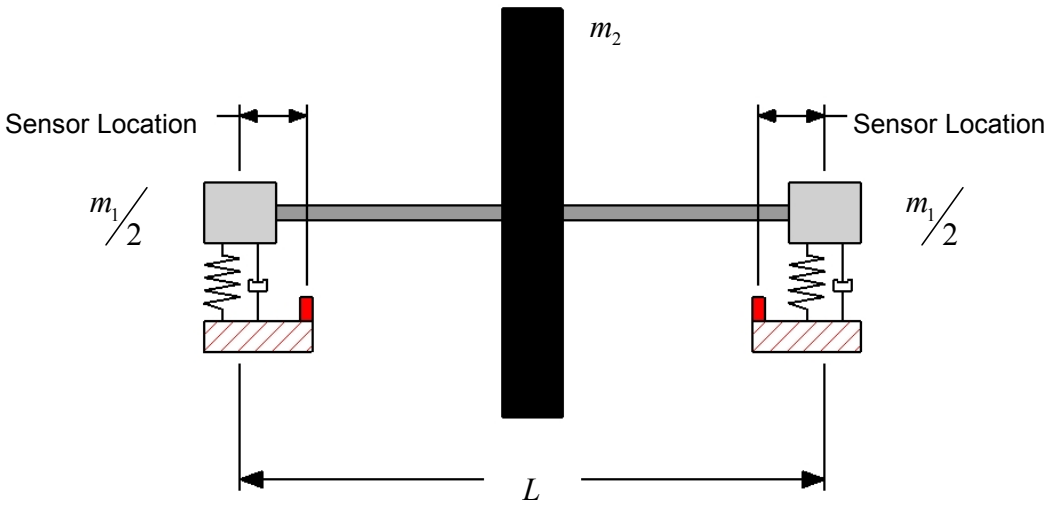

Figure 3.1 Modified Jeffcott rotor on active magnetic bearings

The modified Jeffcott rotor takes the analysis one step further by assuming that the shaft contains mass. This additional mass is added at the bearing locations. Furthermore, the rotor is assumed to be supported by active magnetic bearings that have stiffness and damping. Figure 3.1 shows the modified Jeffcott rotor. In this case, the disc is shown at the mid-span of the shaft of length L and its mass is denoted by m_2. The shaft mass is denoted by m_1 and it is split equally at the bearings. These supports are active magnetic bearings that have stiffness and damping as opposed to rigid supports as is in the case of the standard Jeffcott rotor. Since the modified Jeffcott rotor will be used to study the effects of non-collocation, the sensor locations are shown to be at a location different than the bearing centers.

3.2 Equations of Motion

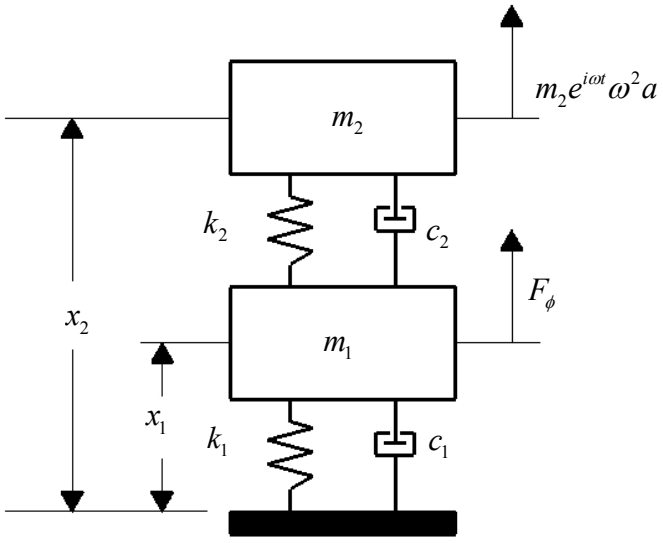

Figure 3.2 Simplified representation of the modified Jeffcott rotor

The system shown in Fig. 3.1 is considered to be symmetrical; therefore, it can be simplified as a two degree-of-freedom problem as shown in Fig. 3.2. This simplified system has two equations of motion. Equations (3.1) and (3.2) are derived from the free body diagram and the application of Newton's Second Law of motion as was done in the previous chapter.

$$m_2\ddot{x}_2 + c_2\dot{x}_2 + k_2x_2 = m_2\omega^2 ae^{i\omega t} + c_2\dot{x}_1 + k_2x_1 \tag{3.1}$$

$$m_1\ddot{x}_1 + c_2\dot{x}_1 + k_2x_1 = F_\phi e^{i\omega t} + c_2\dot{x}_2 + k_2x_2 - c_1\dot{x}_s - k_1x_s \tag{3.2}$$

where,

$$\begin{aligned} x_s &= x_1 + (x_2 - x_1)\sin(\pi\alpha/2) \\ \alpha &= z_s/(L/2) \end{aligned} \tag{3.3}$$

z_s defines the location of the sensor relative to the bearing location and α defines the ratio between the sensor offset and the shaft half-span. In Eq. (3.1), there is an unbalance force acting on m_2 and it is denoted by $m_2\omega^2 ae^{i\omega t}$, where ω is the angular velocity of the rotor and a is the mass eccentricity of unbalance. Since there are magnetic bearings supporting the rotor, there is a constant magnitude force acting on the rotor denoted by $F_\phi e^{i\omega t}$ in Eq. (3.2). This force is necessary because the rotor is assumed to be levitated. The deflection measured at the sensor location is denoted by x_s and it is comprised of two terms. The first term is the deflection of the rotor at the bearing location and the second term is the difference between the deflection at the disc and the deflection of the rotor at the bearing location multiplied by the mode shape. The mode shape is assumed to be a half-period of a sine wave. This assumption allows the sensor deflection to be calculated for varying sensor positions.

Substituting Eq. (3.3) into (3.1)-(3.2) and writing in matrix form yields the following:

$$(X)\begin{pmatrix}\ddot{x}_1\\ \ddot{x}_2\end{pmatrix}+(Y)\begin{pmatrix}\dot{x}_1\\ \dot{x}_2\end{pmatrix}+(Z)\begin{pmatrix}x_1\\ x_2\end{pmatrix}=\begin{pmatrix}F_\phi e^{i\omega t}\\ m_2\omega^2 a e^{i\omega t}\end{pmatrix} \tag{3.4}$$

where,

$$X=\begin{pmatrix}m_1 & 0\\ 0 & m_2\end{pmatrix},\ Y=\begin{pmatrix}c_1(1-\beta)+c_2 & c_1\beta-c_2\\ -c_2 & c_2\end{pmatrix},\ Z=\begin{pmatrix}k_1(1-\beta)+k_2 & k_1\beta-k_2\\ -k_2 & k_2\end{pmatrix}$$

Assuming the solution of $x = Xe^{i\omega t}$, Eq. (3.4) can be written as the following:

$$\begin{pmatrix}A_{11} & A_{12}\\ A_{21} & A_{22}\end{pmatrix}\begin{pmatrix}X_1\\ X_2\end{pmatrix}=\begin{pmatrix}F_\phi\\ m_2\omega^2\end{pmatrix} \tag{3.5}$$

where,

$$\begin{aligned}
A_{11} &= (k_1(1-\beta)+k_2-m_1\omega^2)+i\omega(c_2+c_1(1-\beta))\\
A_{12} &= (k_1\beta-k_2)+i\omega(c_1\beta-c_2)\\
A_{21} &= -k_2-i\omega c_2\\
A_{22} &= (k_2-m_2\omega^2)+i\omega c_2\\
\beta &= \sin(\pi\alpha/2)
\end{aligned}$$

3.3 Effect of Non-Collocation on Critical Speeds

The critical speeds of the modified Jeffcott rotor can be found from Eq. (3.5). Since critical speeds depend on mass and stiffness, the damping terms, c_1 and c_2, are assumed to be zero. Solving for the determinant yields:

$$\omega^4+\left[(1-\beta)\frac{k_1}{m_1}+\frac{(m_1+m_2)}{m_1m_2}k_2\right]\omega^2+\frac{k_1k_2}{m_1m_2}=0 \tag{3.6}$$

It is useful to reduce Eq. (3.6) to Eq. (3.7), which is a non-dimensional form, because the results are more clearly shown.

$$\Omega^2 - \left[1 + \frac{1}{M}(1 + K(1-\beta))\right]\Omega + \frac{K}{M} = 0 \tag{3.7}$$

where,

$$M = m_1 / m_2$$
$$K = k_1 / k_2$$
$$\Omega = \frac{\omega^2}{(k_2 / m_2)}$$

By setting, $M = 1$, and plotting the critical speed, $\frac{\omega}{\sqrt{k_2 / m_2}}$, versus the stiffness ratio, K, on a logarithmic scale yields Fig. 3.3.

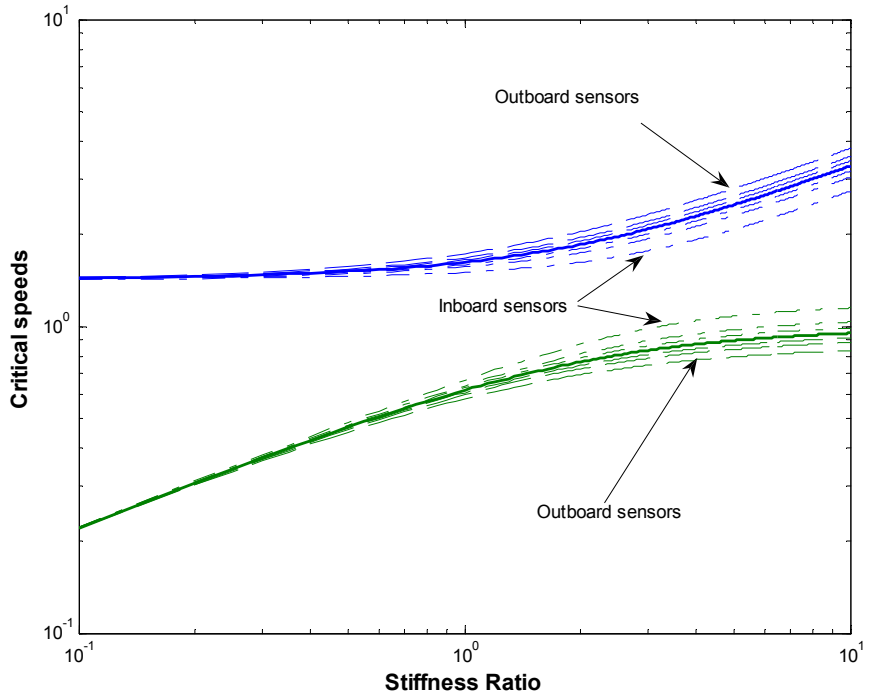

Figure 3.3 Critical speed map of the modified Jeffcott Rotor at M = 1

Figure 3.3 shows the effects of moving the sensor away from the actuating force. For this plot, the sensor is assumed to be moved 20% of the half-span in both directions from the actuating force. The solid line indicates a collocated system, the dashed line indicates the sensors being outboard of the bearings, and the phantom line shows the result when the sensors are moved inboard of the bearings. This figure shows that the first critical speed increases when the sensors are moved inboard, but decreases the second critical speed. The exact opposite is true when the sensors are moved outboard. The first critical speed decreases while the second critical speed increases. This is explained by the first and second mode shapes of the system. Figure 3.4 shows the assumed first and second mode shapes. Figure 3.2 helps to explain these mode shapes. Since this system has been simplified to a two mass system, there are two modes. The first mode occurs when both masses are in phase and the second occurs when they are out of phase. Figure 3.4 shows both modes starting and ending at a deflection of 1. This represents the maximum deflection of m_1. Then the first mode rises to a deflection of 2. This represents a positive maximum deflection of m_2 and shows both masses being in phase. The second mode shows the deflection of m_2 going to 0. This represents a negative maximum deflection of m_2 and shows both masses being out of phase. The first mode takes the form of $X = A\sin(\pi z_s / L) + x_1$, and the second mode is described by $X = x_1 - B\sin(\pi z_s / L)$. This shows that an outside sensor would detect less deflection on the first mode and more deflection on the second mode. Similarly, an inside sensor would detect more deflection on the first mode and less deflection on the second mode.

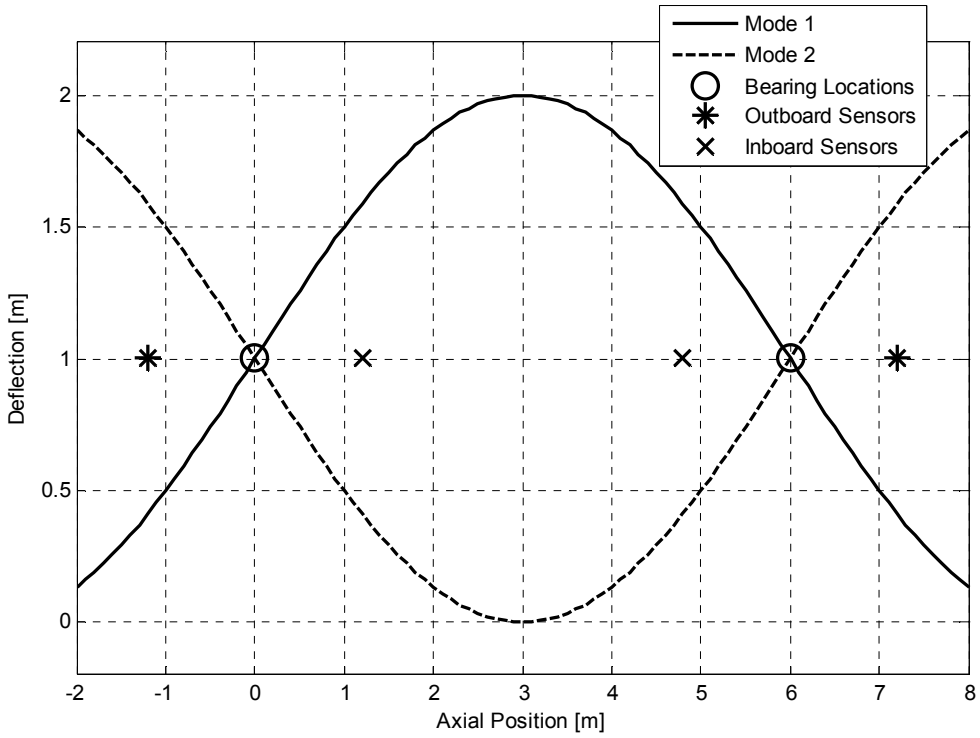

Figure 3.4 Assumed first and second modes shapes and locations of bearings and sensors of modified Jeffcott rotor

Another important thing to note on Fig. 3.3 is the effect of the stiffness ratio. The stiffness ratio is $K = k_1/k_2$, where k_1 is the stiffness of the bearings and k_2 is the stiffness of the flexible rotor. When the ratio is small, the effects of non-collocation are negligible. However, the effects quickly magnify as the stiffness ratio is increased. This is explained by relative deflections. If the shaft has much more stiffness than the bearings, then the position of the sensors becomes less important because the sensors will detect nearly the same deflection. The system will behave more rigidly. However, if the bearings have the same or more stiffness than the shaft, then the sensors will be less accurate the farther away they are from the actuating location.

Figure 3.3 shows the behavior of critical speeds as the sensors are moved relative to the actuating force assuming the mass ratio, $M = 1$. Figure 3.5 shows the same behavior of critical speeds when the mass ratio, $M = 0.2$. At this mass ratio, the center disc has five times more mass than the mass at the bearings. This plot is very similar to Fig. 3.3. Since these two figures are similar, the effects of non-collocation are not dependent on the relative masses.

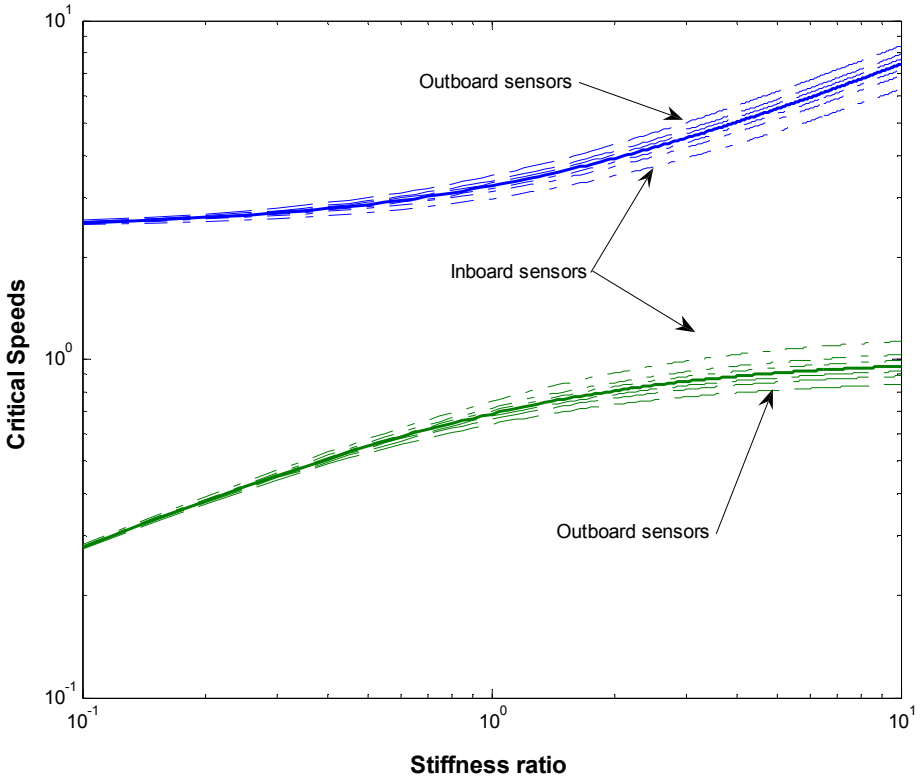

Figure 3.5 Critical speed map of the Modified Jeffcott rotor at M = 0.2

3.4 Summary

While the Jeffcott rotor is a simple system, it offers much insight into complicated systems. Modifying the Jeffcott rotor to include active magnetic bearings allows the effects of non-collocation to be seen and studied. It is important to note that the effects of

non-collocation do not actually change any of the system's characteristics. It does, however, change the control system's interpretation of the system. This occurs because the sensors measure a different deflection than is really occurring at the active magnetic bearings. This has the effect of shifting the critical speeds. A control system designer must take these effects into account to properly control their system [Kirk].

CHAPTER IV

AMB HIGH-SPEED MACHINING SPINDLE ROTOR

4.1 Introduction

The spindle used in this investigation is shown in Fig. 4.1. It is a high speed tool machine spindle supported on active magnetic bearings originally developed by Revolve Magnetic Bearings, a subsidiary of SKF, Inc.

Figure 4.1 AMB supported high speed tool machine spindle

Figure 4.2 Rotor Assembly

The rotor assembly is shown in Fig. 4.2. Typically motors are thought of as an independent or a separate part that consists of a stator and a rotor. However, this rotor has the motor rotor built into it. This is achieved by stacking iron rings between eight copper rings, four on each side. One steel ring is then placed outside the copper rings. The copper rings are clearly shown in Fig 4.2. Then copper rods are pressed axially into these rings.

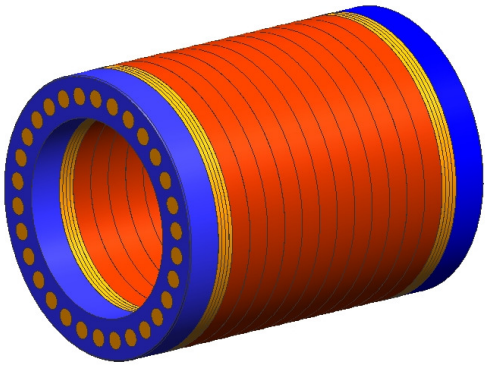

Figure 4.3 Motor construction

Figure 4.3 is a 3D representation of the motor. This motor assembly is then pressed onto the rotor and ground to tight tolerances. The exact construction of the motor is confidential and would not be divulged by SKF.

The rotor assembly also consists of two magnetic bearing journals with lamination stacks and a thrust bearing disk. This rotor assembly is 0.464 meters in length and weighs 6.85 kilograms when the tool holder is attached.

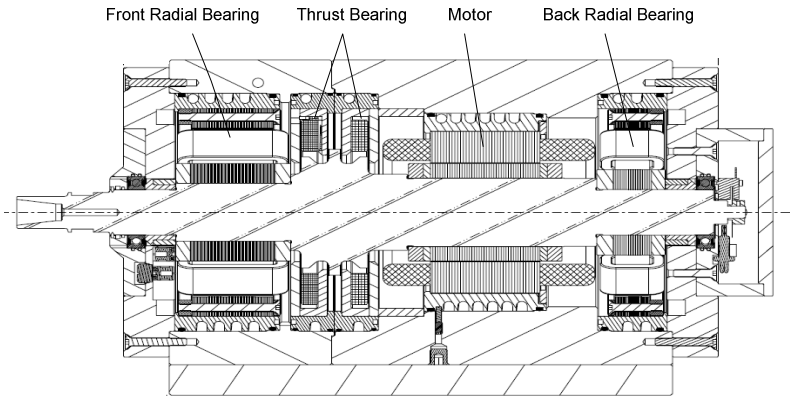

Figure 4.4 Cross-section of the spindle assembly without the tool holder

Figure 4.4 shows a cross-section of the spindle assembly. The machine tool would be attached to the spindle assembly on the left hand side. The spindle is supported by a front radial bearing with a static load capacity of 1400 N and a rear radial bearing capable of 600 N. Axial loads are handled by the thrust bearing which is capable of 500 N of maximum axial force. The spindle has a maximum speed of 50,000 rpm at 10 kW.

4.2 Model of Spindle Rotor

A finite element model was created of the spindle. This model has 64 nodes and 63 elements. The model also contains a machine tool holder that is 64.95 millimeters in length. The 63 elements are shown in Fig. 4.5. This model is not an exact copy of the actual rotor, but it is a close approximation. Also, the analysis assumes a free-free rotor. A free-free rotor assumes the system has no supports. This would be nearly the same as suspending the actual rotor with wires and applying an impulse load with a hammer.

This assumption is valid because the rotor's system characteristics are of interest and not the stiffness and damping of the supports.

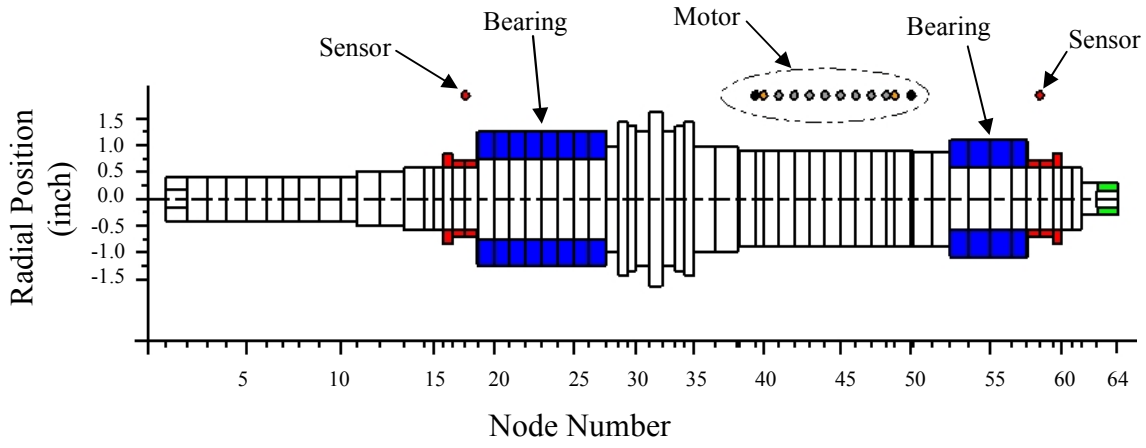

Figure 4.5 FEA model of high-speed machining spindle

Another model will also be examined using a different FEA software. This software is capable of handling the complete detailed model. In this analysis, the rotor will be broken down into approximately fifty-two thousand elements. The results of this model will be compared to the previous model to gauge the accuracy of the reduced model. Even though, this model will be as accurate as possible, there will still be some inaccuracies inherent to computer modeling. These will be discussed in the proceeding sections.

4.3 Rotordynamic Analysis Versus Experimental Results

4.3.1 Detailed Model Analysis

The rotordynamic analysis will begin with the detailed model. The model used in this analysis is shown in Fig. 4.6, where the rotor assembly is shown by the different materials. The material properties are listed in Appendix A.

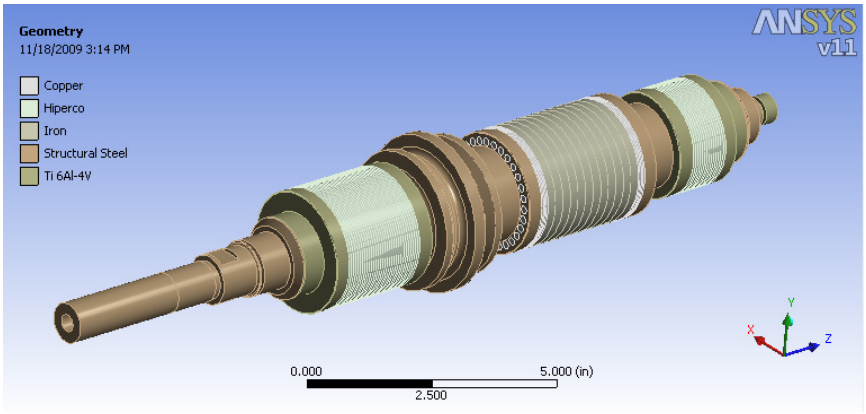

Figure 4.6 Detailed model of rotor assembly

As was previously stated, this model contains more detail than the reduced model and it will be used to gauge the accuracy of the reduced model. Furthermore, the results will provide insight so that the reduced model will be reduced in the proper manner. For all analyses, the first four modes will be studied. These include two rigid body modes and the first two flexible modes.

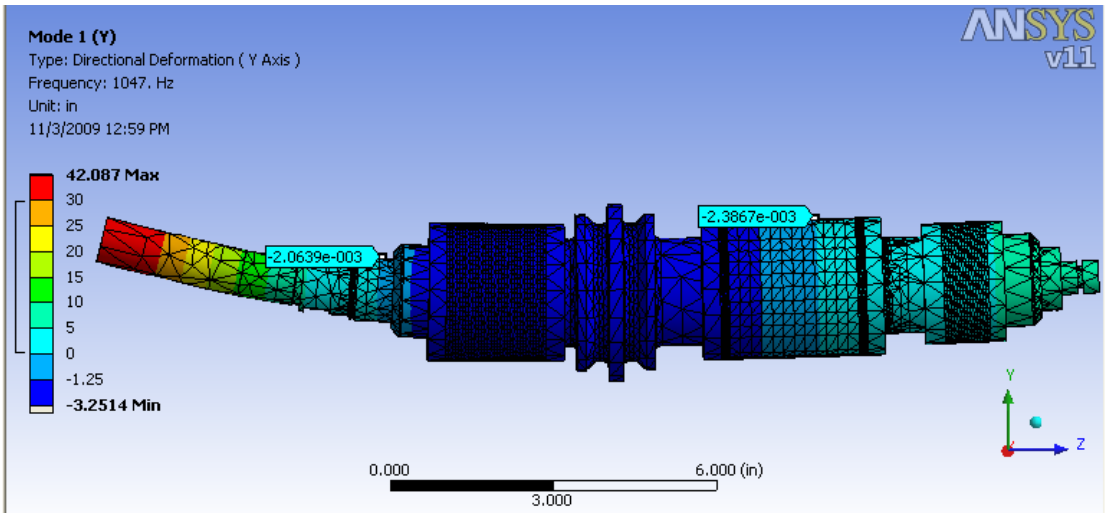

Figure 4.7 First flexible mode shape of the detailed model

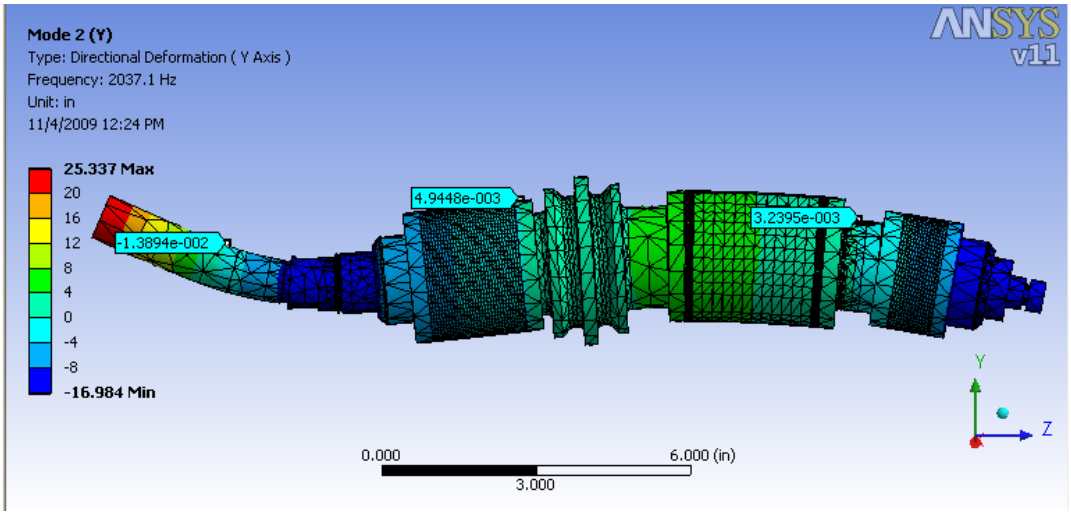

Figure 4.8 Second flexible mode shape of the detailed model

Figures 4.7 and 4.8 are the first and second mode shapes. The first natural frequency is shown to be approximately 1047 Hz with the nodes of the first mode at approximately 5.060 and 13.100 inches. The second natural frequency is found to be 2037 Hz. The nodes of the second mode are found to be at 2.250, 8.150 and 14.600

inches. It should be noted that the displacements shown in Figs. 4.7 and 4.8 are relative and not absolute.

Upon closer examination of the results, an interesting detail is found. As was previously mentioned, the motor and bearings are not one piece but contain many laminations. Figure 4.9 shows a close up view of the motor laminations for the second mode. This view shows gaps between the laminations. Even though they are small, they provide valuable insight for the reduced model. When reducing the model, two approaches can be taken. The first approach is to model the laminations as part of the main rotor and then compensating for the different materials in the density and Young's Modulus. The second approach is to model the main rotor and add the laminations of the bearings and motor as added masses and then add the correct inertias to the masses. Figure 4.9 shows the second approach to be correct for the motor. Since there are thirty copper rods through the laminations, the assumption will be that the rods are pressed through the laminations. This will be shown as the laminations being bonded to the rods, but not each other. The bearings are handled a little differently because there are no rods through them. They are modeled as being bonded together. This would make sense from an assembly point of view because the bearing laminations are known to be very thin.

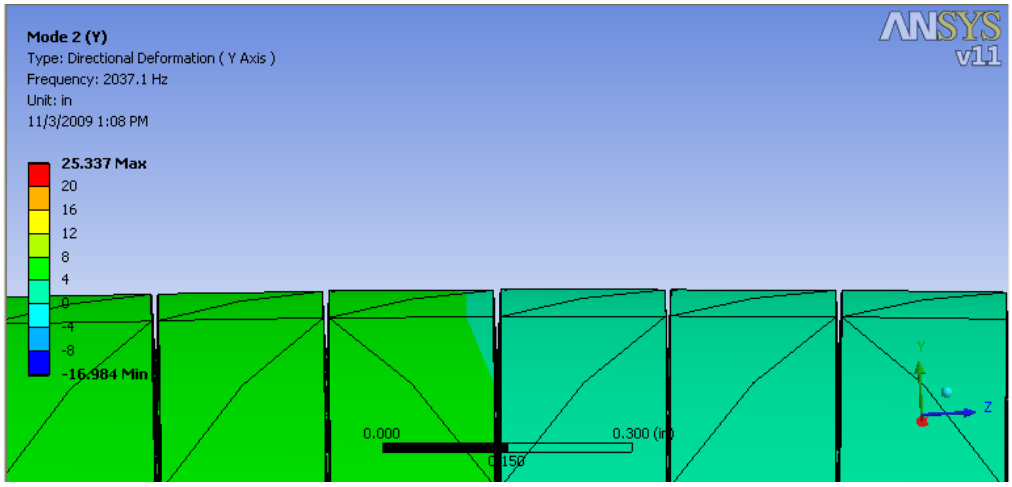

Figure 4.9 Close up view of the motor in the second mode shape of the detailed model

4.3.2 Reduced Model Analysis

As was stated a previous section, the reduced model contains 63 elements. The bearings and motor are modeled in a similar way as the detailed model. With this software, the difference is that the bearings are assumed to be part of the main rotor. With this assumption, the density and Young's modulus are modified based on the volume for each material. On the other hand, the motor will be modeled as twelve added masses. Since the diameters are known, the correct moment of inertias will be added to make the model as correct as possible. The complete input file can be found in Appendix B. Figure 4.10 illustrates the first and second flexible mode shapes. This software returned natural frequencies of 1109 Hz and 1978 Hz. This reflects a difference of 6% and 3%, respectively, from the detailed model. The nodes of the mode shapes are also shown, and they are in close agreement with the detailed model. Based on these two facts, the reduced model is a valid representation of the spindle.

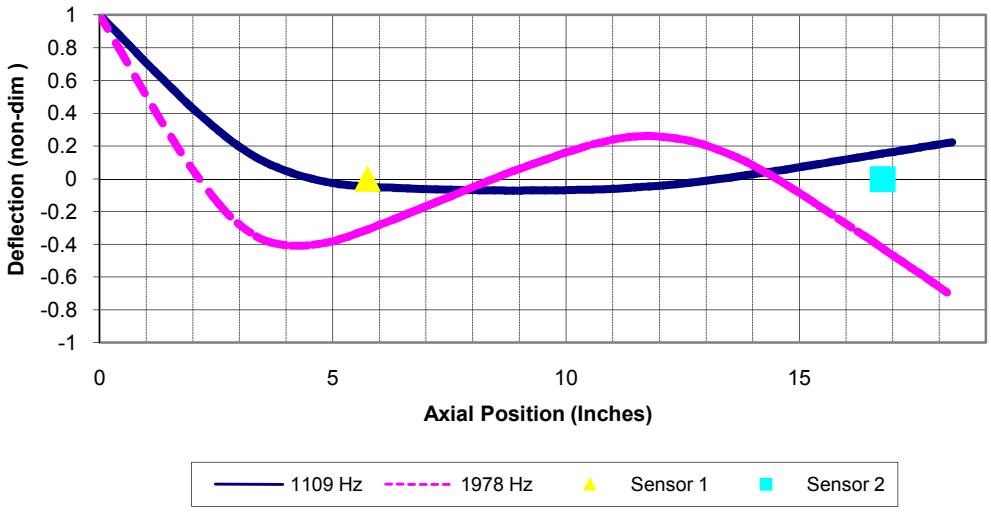

Figure 4.10 First and second mode shapes of the reduced model

The reduced model is necessary because each element has two degrees of freedom. Each degree of freedom leads to an equation of motion. Therefore, a 63 element model will have 126 equations of motion, while a fifty-two thousand element model will contain 104,000 equations of motion. It simply is not practical to solve that many equations, and therefore, the number must be reduced. As long as the model is reduced properly, very little will be lost and the results will be valid.

4.3.3 Experimental Analysis Results

An experiment was conducted to measure the open loop transfer function of the levitated rotor. The PID controller utilized dSPACE based on differential control for the experiment. The hardware consisted of the DS1005 PPC Board featuring the PowerPC 750GX. The sampling time of the controller was 10 kHz. This system has four inputs and four outputs. Each of the two active magnetic bearings have two input signals, one

for each of the x- and y- planes. The four output signals of the system are the sensor signals of the x- and y- planes of the front and rear sensors. Therefore, the open loop transfer function would take the form:

$$\begin{Bmatrix} y_1 \\ y_2 \\ y_3 \\ y_4 \end{Bmatrix} = G(s) \begin{Bmatrix} u_1 \\ u_2 \\ u_3 \\ u_4 \end{Bmatrix} \tag{4.1}$$

where, $G(s)$ is a 4 x 4 matrix of transfer functions relating each input to each output. $G(s)$ can be measured by performing four experiments; however, there are only two transfer functions of interest. Therefore, two experiments are performed. These two transfer functions are $G(1,1)$ and $G(3,3)$. $G(1,1)$ relates the output of the front sensor to an input at the front bearing and $G(3,3)$ relates the output of the rear sensor to an input at the rear bearing. The input and output will be in the x- plane for both cases. In each experiment, one input is perturbed individually and one output is measured and recorded. The perturbation is a sinusoidal signal that sweeps the desired frequencies with a current of 0.25 Ampere. In this case, the first and second modes are of interest; therefore, the frequency range is 0 to 2500 Hz. By following this methodology, the input and output signals are related by:

$$Y(\omega_i) = G(j\omega_i)U(\omega_i) \tag{4.2}$$

Therefore, the transfer function is:

$$G(j\omega_i) = U^{-1}(\omega_i)Y(\omega_i) \tag{4.3}$$

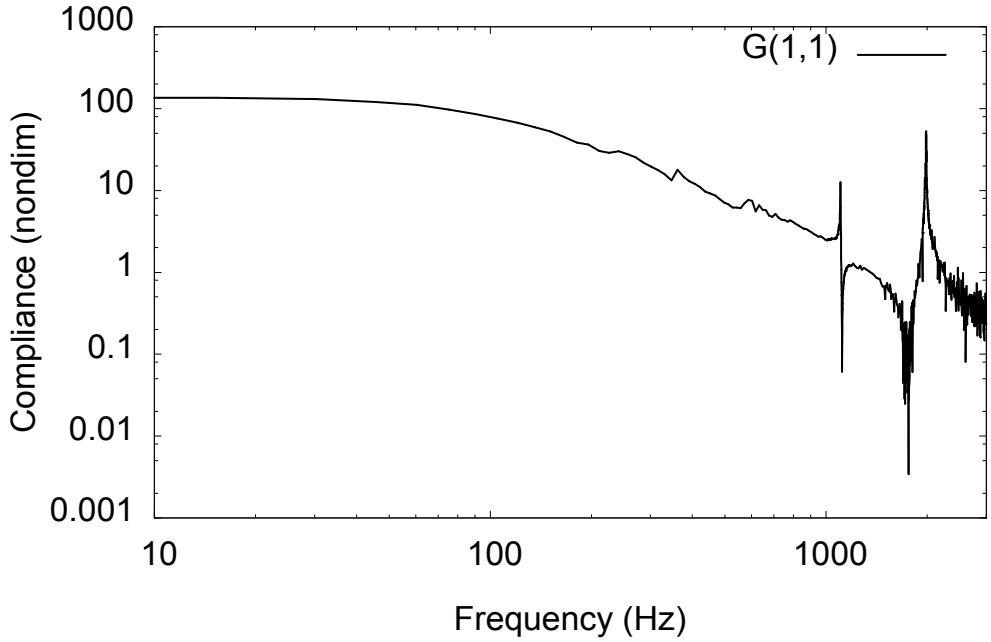

Figure 4.11 Open loop transfer function, G(1,1)

Figure 4.11 shows the results from the first experiment. In this case, the sinusoidal perturbation was applied to the front bearing, the bearing closest to the tool holder, and the output was at the front sensor. These results show two resonant frequencies at approximately 1100 Hz and 1950 Hz and two anti-resonant frequencies at approximately 1100 Hz and 1800 Hz. If this were a collocated system, there would only be one anti-resonance between two consecutive resonances. However, this is not the case and there are two anti-resonances between consecutive resonances. This is explained by the mode shapes. In Fig. 4.10, the node of the first mode comes right before the sensor and actuator. Figure 4.11 illustrates this with a resonance and anti-resonance at nearly the same frequency.

Another interesting point is the magnitude of the first resonant frequency. The magnitude is relatively small. This is also a result of the sensor being in close proximity

to the node of the mode shape. When a sensor is near the node of a mode shape, the sensor will see little deflection. This manifests itself as a small magnitude in the resonant frequency of that particular mode. If the node existed at the exact same location as the sensor, the resonant frequency would not be identifiable. This is a unique problem of non-collocated systems. If a control system designer had to identify the natural frequencies of a non-collocated system and there was a node located near the sensor, then that natural frequency might be missed. This could cause major issues in operation.

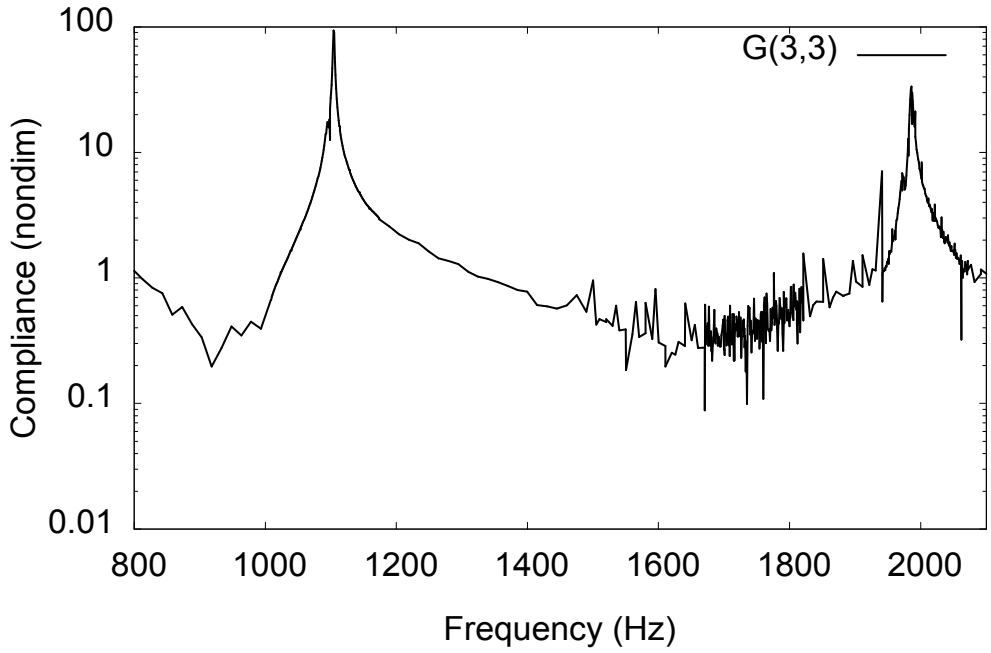

Figure 4.12 Open loop transfer function, G(3,3)

Figure 4.12 illustrates the results of the open loop transfer function when the sinusoidal perturbation is injected into the back bearing with the output coming from the back sensor. As expected, the resonances are in close agreement with Fig. 4.11, but the anti-resonances are not. The anti-resonances or zeros, are not easily identified, but are located at roughly 950 Hz and 1750 Hz. They are not close to the resonances, which

suggests there is no node nearby. This is also agrees with the mode shapes plot of Fig. 4.10. The first resonance, while at the same frequency of approximately 1100 Hz, is much more pronounced with a higher magnitude. Without a node nearby, it is shown as expected.

4.4 Summary

Active magnetic bearings offer some great advantages to a multitude of industries including high speed machining [Sawicki 2008]. However, due to their non-collocated nature, they also offer some challenges. The first step in understanding how to control them properly is developing an accurate model. This takes much time and understanding of the particular system. Mistakes in creating the model can lead to instability and/or uncontrollability. Also it is important to control the size of the model. A very large model might be very accurate, but too large to solve. On the other hand, a model that was reduced too much or in an improper way, can lead to inaccuracies. The latter situation is solvable, but the results are not valid. Once the accurate model is created, the resonant frequencies and mode shapes can be extracted. The dangers of running a system at a resonant frequency are very well known. However, the locations of the zeros in relation to the mode shapes can be just as problematic.

In this particular high speed machining spindle system, a detailed model was created and the resonant frequencies and mode shapes were shown. This created the benchmark for the reduced model to attain. The presented reduced model was very close on returning the correct resonances and mode shapes for the first two flexible modes. Finally, the experiments were performed and the results were presented. The results of

the experiments were in close agreement with both models. Furthermore, the issues of non-collocation were clearly shown in the results of the experiments. It was shown how non-collocation can reduce the magnitude of a resonant frequency. The magnitude could be reduced to the point that it essentially erases a resonant frequency. In some cases this can be positive, but only if the control system designer recognizes the fact that a resonant is missing. If this is not recognized and the missing resonant occurs within the operating range of the system, the control system will not function properly and there is potential for damage to equipment. Non-collocated systems are not necessarily undesirable systems, but extra care must be taken to fully account for the differences.

CHAPTER V

CONCLUSIONS

5.1 Summary

Technologies that utilize non-collocated systems such as active magnetic bearings and robotics are becoming more and more prevalent. These systems present the control system designer with some challenges. These challenges were shown in a variety of theoretical examples from a simple two-mass system, a more complicated flexible beam system, to a modified Jeffcott rotor. From there, a real-life example of a non-collocated system was analyzed. This system consisted of a rotor with a single disc and two conical magnetic bearing rotors. The results were presented and the differences between a collocated system and non-collocated system were illustrated. Finally, a high-speed machining spindle supported by active magnetic bearings was analyzed. The importance of an accurate model was shown and this system demonstrated some challenges of non-collocation. The major issue was found to be in identifying resonant frequencies. If the

resonant frequencies are not identified properly and they are within the operating range of the system, the system will not function properly and possible damage can occur. The damage to parts in the system can be expensive and it will cause the system to experience downtime for repair.

Non-collocation affects the zeros of the system. The amount of the effects are dependent on the distance between the sensor and actuator. It was shown that zeros play a key role in determining the stability of a system. It was also shown that the poles, or natural frequencies, of a system are not dependent on sensor location. The poles are only dependent on the dynamics of the system, notably mass and stiffness. Control system designers are well aware of the importance of natural frequencies or poles, but the zeros can be overlooked. Understanding the zeros and their interaction with the mode shapes of a system is crucial in designing a robust control system.

Overall non-collocated systems can be more difficult to control than a comparable collocated system due to stability concerns. However, all these challenges can be overcome if the system designer understands the issues and plans accordingly.

5.2 Further Research Directions

This thesis examined the differences between a collocated and non-collocated system through a wide variety of examples and a case study involving a high-speed machining spindle. The challenges of controlling these non-collocated systems were presented. It would be recommended for a control system designer to study different ways of overcoming the presented challenges. Although some techniques have been studied, more work is required in this area. Showing how a control system would differ

between a collocated system and a similar non-collocated system would be interesting, and this could prove to be valuable for technologies that are inherently non-collocated to be more widely accepted.

BIBLIOGRAPHY

Bischof, K.R., 2002, "Dynamics and Control of Magnetically Levitated High-Speed Rigid Rotor to Produce N-Waved Orbits", Dissertation, Cleveland State University, Cleveland, OH, USA.

Bruin, J.C.A., Doris, A., Wouw, N., Heemels, W.P.M.H, Nijmeijer, H., 2008, "Control of a Mechanical Motion Systems With Non-Collocation of Actuation and Friction: A Popov Criterion Approach for Input-To-State Stability and Set-Valued Nonlinearities", *Automatica*, Vol. 45, pp. 405-415.

Buhr, C., Franchek, M.A., Bernhard, R.J., 1997, "Non-Collocated Adaptive-Passive Vibration Control", *Journal of Sound and Vibration*, Vol. 206, pp. 371-398.

Damaren, C.J., 2000, "Passivity and Noncollocation in the Control of Flexible Multibody Systems", *Journal of Dynamic Systems, Measurement, and Control*, Vol. 122, pp. 11-17.

Ginsberg, J.H., 2001, *Mechanical and Structural Vibrations*, John Wiley & Sons, Inc. New York.

Guo, B.Z., Wang, J.M., Yang, K.Y., 2008, "Dynamic Stabilization of an Euler-Bernoulli Beam Under Boundary Control and Non-Collocated Observation", *Systems & Control Letters*, Vol. 57, pp. 740-749.

Guo, B.Z., Shao, Z.C., 2008, "Stabilization of an Abstract Second Order System With Application to Wave Equations Under Non-Collocated Control and Observations", *Systems & Control Letters*, Vol. 58, pp. 334-341.

Kirk, R.G., Keesee, J., Rawal, D., "Critical Speeds and Forced Response Solutions of Active Magnetic Bearin Turbomachinery, Part 1", Virginia Polytechnic Institute and State University, Blacksburg, VA, USA, pp. 539-558.

Lacarbonara, W., Yabuno, H, Hayashi, K., 2006, "Non-linear Cancellation of the Parametric Resonance in Elastic Beams: Theory and Experiment", *International Journal of Solids and Structures*, Vol. 44, pp. 2209-2225.

Loix, N., Kozanek, J., Foltete, E., 1996, "On the Complex Zeros of Non-Collocated Systems", *Journal of Structural Control*, Vol. 3, pp. 79-87.

Martin, G.D., 1978, "On the Control of Flexible Mechanical Systems", Dissertation, Stanford University, Palo Alto, CA, USA.

Maslen, E.H., 1995, "Positive Real Zeros in Flexible Beams", *Shock and Vibration*, Vol. 2, No. 6, pp. 429-435.

Miu, D.K., 1991, “Physical Interpretation of Transfer Function Zeros for Simple Control Systems with Mechanical Flexibilities”, *Journal of Dynamic Systems, Measurement, and Control*, Vol. 113, pp. 419-424.

Nordstrom, L., Nordberg, P., 2004, "A Time Delay Method to Solve Non-Collocated Input Estimation Problems", *Mechanical Systems and Signal Processing*", Vol. 18, pp. 1469-1483.

Preumont, A., 2002, *Vibration Control of Active Structures An Introduction*, Kluwar Academic Publishers.

Qiu, Z., Han, J., Zhang, X., Wang, Y., Wu, Z., 2009, "Active Vibration Control of a Flexible Beam Using a Non-Collocated Acceleration Sensor and Piezoelectric Patch Actuator", *Journal of Sound and Vibration*, Vol. 326, pp. 438-455.

Richelot, J., Bordeneuve-Guibe, J., Pommier-Budinger, V., 2004, "Active Control of a Clamped Beam Equipped with Piezoelectric Actuator and Sensor Using Generalized Predictive Control", *IEEE International Symposium on Industrial Electronics*, Montreal, Canada, 24-27 August.

Sawicki, J.T., Maslen, E.H, 2007, “Rotordynamic Response and Identification of AMB Machining Spindle”, *ASME Turbo Expo 2007: Power for Land, Sea, and Air*, Montreal, Canada, 14-17 May.

Sawicki, J.T., Maslen, E.H, Bischof, K.R., 2006, “Modeling and Performance Evaluation of Machining Spindle with Active Magnetic Bearings”, *The 8th International Conference on Motion and Vibration Control*, KAIST Daejong campus, South Korea, 28-30 August.

Sawicki, J.T., Maslen, E.H., 2008, “Accurate Identification of Plant Model for Robust Control of an AMB Machine Tool Spindle”, *The 9th International Conference on Motion and Vibration Control*, Technische Universitaet Muenchen, Germany, 15-18 September.

Spector, V.A., Flashner, H., 1989, “Sensitivity of Structural Models for Noncollocated Control Systems”, *Journal of Dynamic Systems, Measurement, and Control*, Vol. 111, pp. 646-655.

Spector, V.A., Flashner, H., 1990, “Modeling and Design Implications of Noncollocated Control in Flexible Systems”, *Journal of Dynamic Systems, Measurement, and Control*, Vol. 112, pp. 186-193.

Sun, D., Tong, L., Atluri, S.N., 2001, "Effects of Piezoelectric Sensor/Actuator Debonding on Vibration Control of Smart Beams", *International Journal of Solids and Structures*, Vol. 38, pp. 9033-9051.

Vance, J.M., 1988, *Rotordynamics of Turbomachinery*, John Wiley & Sons, Inc. New York.

Zelinski, P., 2008, “No Need for Speed”, *Modern Machine Shop*, Vol. 80, No. 10, pp. 79-85.

APPENDICES

APPENDIX A

High - Speed Machining Spindle Material Properties

Material	Density (lb/in^3)	Young's Modulus (ksi)	Poisson's Ratio (dimensionless)
4140 Steel	0.284	29,700	0.290
Copper	0.323	16,000	0.343
Hiperco 50 Fe-Co-V	0.293	30,000	0.291
Iron	0.284	29,000	0.291
Titanium Ti-6Al-4V	0.160	16,500	0.330

APPENDIX B

Model Input File

```
High Speed Machining Spindle Model
Tim Obrzut, November 1, 2009
0          0.4170 0.8268 0.2165 0       0       29.7    0.2840 0 0 0 0
0.         0.3800 0.8268 0.     0       0       29.7    0.2840 0 0 0 0
0          0.3800 0.8268 0.     0       0       29.7    0.2840 0 0 0 0
0          0.3800 0.8268 0.     0       0       29.7    0.2840 0 0 0 0
0          0.3800 0.8268 0.     0       0       29.7    0.2840 0 0 0 0
0          0.6300 0.8268 0.     0       0       29.7    0.2840 0 0 0 0
0.         0.3937 0.8268 0.     0       0       29.7    0.2840 0 0 0 0
0          0.3937 0.8268 0.     0       0       29.7    0.2840 0 0 0 0
0          0.3150 0.8249 0      0       0       29.7    0.2840 0 0 0 0
0          0.4528 1.0236 0      0       0       29.7    0.2840 0 0 0 0
0          0.4528 1.0236 0      0       0       29.7    0.2840 0 0 0 0
0          0.3937 1.1654 0      0       0       29.7    0.2840 0 0 0 0
0          0.1772 1.1654 0      0       0       29.7    0.2840 0 0 0 0
0          0.1850 1.1654 0      0       0       29.7    0.2840 0 0 0 1
0          0.1791 1.6929 0      0       0       30.0    0.2840 0 0 0 0
0.         0.2411 1.4173 0      0.      0.      30.0    0.2840 0 0 0 0
0.05192    0.2411 1.4173 0      0.      0.      30.0    0.2840 0 1 0 0
0.         0.3150 2.5197 0      0.      0.      25.3    0.2336 0 0 0 0
0.         0.3051 2.5197 0      0.      0.      30.0    0.2877 0 0 0 0
0.         0.3051 2.5197 0      0.      0.      30.0    0.2877 0 0 0 0
0.         0.3051 2.5197 0      0.      0.      30.0    0.2877 0 0 0 0
0.         0.3051 2.5197 0      0.      0.      30.0    0.2877 1 0 0 0
0.         0.3051 2.5197 0      0.      0.      30.0    0.2877 0 0 0 0
0.         0.3051 2.5197 0      0.      0.      30.0    0.2877 0 0 0 0
0.         0.3346 2.5197 0      0.      0.      25.3    0.2336 0 0 0 0
0          0.2264 1.9685 0      0       0       29.7    0.2840 0 0 0 0
0          0.1673 2.8740 0      0       0       29.7    0.2840 0 0 0 0
0          0.1772 2.6969 0      0       0       29.7    0.2840 0 0 0 0
0          0.2461 2.5197 0      0       0       29.7    0.2840 0 0 0 0
0          0.2559 3.2520 0      0       0       29.7    0.2840 0 0 0 0
0          0.2461 2.5197 0      0       0       29.7    0.2840 0 0 0 0
0          0.1772 2.6969 0      0       0       29.7    0.2840 0 0 0 0
0          0.1673 2.8740 0      0       0       29.7    0.2840 0 0 0 0
0          0.4281 1.9685 0      0       0       29.7    0.2840 0 0 0 0
0          0.4281 1.9685 0      0       0       29.7    0.2840 0 0 0 0
0          0.0197 1.7717 0      0       0       29.7    0.2840 0 0 0 0
0.2255     0.3150 1.7717 0      0.0905  0.1356  30.000  0.2840 0 0 0 0
0.1286     0.1575 1.7717 0      0.0516  0.0765  30.000  0.2840 0 0 0 0
0.1682     0.2953 1.7717 0      0.0675  0.1010  30.000  0.2840 0 0 0 0
0.1682     0.2953 1.7717 0      0.0675  0.1010  30.000  0.2840 0 0 0 0
```

0.1682	0.2953	1.7717	0	0.0675	0.1010	30.000	0.2840	0	0	0	0
0.1682	0.2953	1.7717	0	0.0675	0.1010	30.000	0.2840	0	0	1	0
0.1682	0.2953	1.7717	0	0.0675	0.1010	30.000	0.2840	0	0	0	0
0.1682	0.2953	1.7717	0	0.0675	0.1010	30.000	0.2840	0	0	0	0
0.1682	0.2953	1.7717	0	0.0675	0.1010	30.000	0.2840	0	0	0	0
0.1682	0.2953	1.7717	0	0.0675	0.1010	30.000	0.2840	0	0	0	0
0.1286	0.1575	1.7717	0	0.0516	0.0765	30.000	0.2840	0	0	0	0
0.2285	0.3150	1.7717	0	0.0905	0.1356	30.000	0.2840	0	0	0	0
0	0.0394	1.7717	0	0	0	29.7	0.2840	0	0	0	0
0	0.3543	1.7520	0	0	0	29.7	0.2840	0	0	0	0
0	0.3543	1.7520	0	0	0	29.7	0.2840	0	0	0	0
0.	0.3543	2.2047	0	0.	0.	23.6	0.2264	0	0	0	0
0.	0.4134	2.2047	0	0.	0.	29.8	0.2820	0	0	0	0
0.	0.4134	2.2047	0	0.	0.	29.8	0.2820	1	0	0	0
0.	0.2953	2.2047	0	0.	0.	23.6	0.2264	0	0	0	0
0.	0.2461	1.4173	0	0.	0.	30.0	0.2840	0	1	0	0
0.0528	0.2461	1.4173	0.	0.	0.	30.0	0.2840	0	0	0	0
0	0.1772	1.6929	0	0	0	30.0	0.2840	0	0	0	0
0	0.1870	1.1654	0	0	0	29.7	0.2840	0	0	0	0
0	0.1870	1.1654	0	0	0	29.7	0.2840	0	0	0	1
0	0.3004	0.6102	0	0	0	29.7	0.2840	0	0	0	0
0	0.3886	0.6102	0	0	0	29.7	0.2000	0	0	0	0
0	0.	0.1969	0	0	0	00.0	0.0000	0	0	0	0